A survey of computational models for adhesion

Roger A. Sauer [1]

Aachen Institute for Advanced Study in Computational Engineering Science (AICES), RWTH Aachen University, Templergraben 55, 52056 Aachen, Germany

Published[2] in *The Journal of Adhesion*, DOI: 10.1080/00218464.2014.1003210
Submitted on 24. October 2014, Revised on 26. December 2014, Accepted on 26. December 2014

Abstract

This work presents a survey of computational methods for adhesive contact focusing on general continuum mechanical models for attractive interactions between solids that are suitable for describing bonding and debonding of arbitrary bodies. The most general approach are local models that can be applied irrespective of the geometry of the bodies. Two cases can be distinguished: local material models governing the constitutive behavior of adhesives, and local interface models governing adhesion and cohesion at interfaces in the form of traction-separation laws. For both models various sub-categories are identified and described, and used to organize the available literature that has contributed to their advancement. Due to their popularity and importance, this survey also gives an overview of effective adhesion models that have been formulated to characterize the global behavior of specific adhesion problems.

Keywords: bonding and debonding, cohesive zone modeling, contact mechanics, interfaces, mechanical properties of adhesives, numerical analysis

1 Introduction

This survey pursues two aims: (1) to give an overview of the computational methods and the underlying theoretical formulations for adhesion that have been considered in the literature, and (2) to bring structure and classification into the huge range of modeling approaches. Both aims are pursued from the modeling point of view.

There is a huge literature body on works related to computational adhesion, especially when including computational cohesion, which is equivalent from the model standpoint. A search on web of science[3] generates more than 12.000 hits (as of October 2014). And this even misses some of the important works, simply because they do not use those keywords. It is therefore impossible to account for every single publication related to the subject and give a complete overview of all related works. The aim of this survey is to rather give a complete overview of the methods and approaches of computational adhesion with the following focus:

The focus is on computational models and not on analytical and experimental models. A recent overview of theoretical and experimental approaches of the physics of adhesion is given by Gerberich and Cordill (2006). Here, only selected theories are discussed that are relevant for computations.

[1]email: sauer@aices.rwth-aachen.de
[2]This pdf is the personal version of an article whose final publication is available at www.sciencedirect.com
[3]https://webofknowledge.com; search = (computational OR numerical) AND (adhesion OR cohesion)

The focus is on general models that apply to a large range of problems and not on specific models that only apply to few problems, which are, for example, characterized by a special geometry. The focus is thus placed on models that can be adapted to any kind of adhesion mechanism and adherent geometry.
The focus is on continuum models that are typically valid above length scales of several nanometers, while atomistic models and corresponding computations are not discussed in detail even though there is much work in this field, e.g. see Landman et al. (1990) and citations thereof.
The focus is on the mechanical aspects of adhesion, but an overview of the modeling of thermal effects as well as curing and aging is also discussed.
The focus is on adhesion in the sense of attractive forces between neighboring bodies, and not in the sense of tangential sticking between bodies, as is sometimes considered in the literature, e.g. see Mróz and Stupkiewicz (1998).
The focus is on adhesion of solids, while the adhesion of liquids is not discussed in great detail here. However, the computational methods presented here in principle also apply to liquids.

Adhesion originates from various mechanisms. Some of these are only secondary or apparent adhesion effects, since no attractive forces are present locally, but the mechanism still appears adhesive on the global scale. The local modeling of apparent adhesion mechanisms thus does not require an adhesion formulation. Only the global modeling does. The following six mechanism can be distinguished (Comyn, 1997):

- Chemical adhesion, due to strong molecular bonds – like covalent and ionic bonds – or due to weak hydrogen bonds. Chemical adhesion is only of short range, usually less than one nanometer.
- Dispersive adhesion, due to van der Waals interaction. This is a quantum mechanical effect of (momentary) polarity within molecules. It is of longer range, up to several nanometers.
- Electrostatic attraction, due to Coulomb interaction between oppositely charged bodies. This interaction can easily extend beyond the centimeter range.
- Mechanical interlocking of the surfaces, e.g. for a nail in a wall. This is only apparent adhesion since no local tensile interface forces exist, but only local compression and friction forces.
- Diffusive adhesion, due to interlocking at the molecular level, e.g. of polymer chains. Also this is only apparent adhesion.
- Suction. This is apparent adhesion since, physically, no tensile forces are present in the interface. The bodies are rather pressed together by ambient atmospheric pressure.

Further details on the origins of molecular adhesion can be found in Israelachvili (1991). In principle also gravitation and magnetism exert attractive forces. But those are (typically) restricted to celestial length scales and special materials, respectively.

Adhesion plays an important, if not dominating, role in many applications. Examples are debonding and delamination (Allix and Ladevèze, 1992; Point and Sacco, 1996a) – e.g. of thin films (Hendrickx et al., 2005; Roy et al., 2007), peeling of adhesive strips (Kendall, 1975), rubber adhesion (Johnson et al., 1971), adhesion by capillary bridges (Orr et al., 1975), flow and aggregation of adhesive particles (Kendall et al., 2007; Liu et al., 2010; Li et al., 2011b), rough surface adhesion (Persson et al., 2005) and bonding (Hunter et al., 2012), multiscale adhesion modeling (Sauer, 2009b, 2014a; Eid et al., 2011a), adhesive bonding technology (Banea and da Silva, 2009; He, 2011), MEMS and NEMS (Micro- and Nano-electromechanical systems)

(Komvopoulos, 2003; Zhao et al., 2003), insect and lizard adhesion (Autumn and Peattie, 2002; Arzt et al., 2003), climbing robots (Spenko et al., 2008), microfiber arrays (Yurdumakan et al., 2005; Aksak et al., 2007; Ge et al., 2007; Kim et al., 2007; Schubert et al., 2007; Qu et al., 2008), biomimetic and patterned adhesive surfaces (Ghatak et al., 2004; Gorb et al., 2007), self-cleaning mechanisms (Blossey, 2003), biofouling (Tsang et al., 2006), membrane adhesion (Lipowsky and Seifert, 1991; Andrews et al., 2003; Wan and Julien, 2009; Agrawal, 2011), adhesion of cells (Zhu, 2000), and hemostatic platelet adhesion (Wang and King, 2012).

In order to structure this survey we distinguish between the following three modeling approaches for adhesion:
(a) local material models that describe the material behavior within the adhesive (Sec.2),
(b) local interface models that describe the bonding behavior at the material interface (Sec.3),
and (c) global adhesion models that describe the effective adhesion behavior (Sec.4).
Fig. 1 shows a schematic overview of these three approaches. In all cases the adhesion behavior

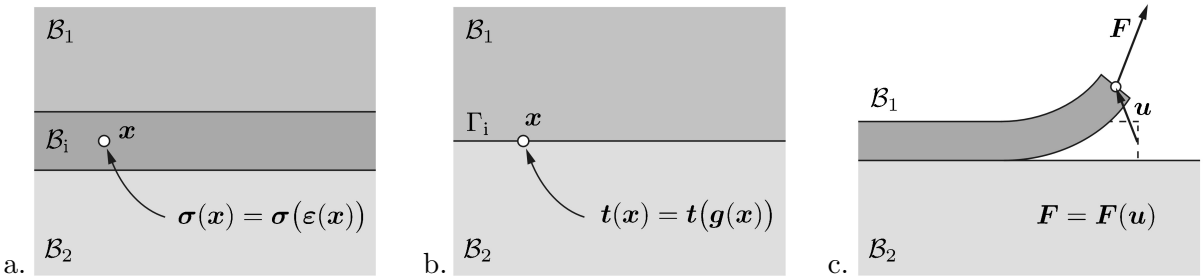

Figure 1: Classification of adhesion models: (a) local material models for adhesives; (b) local interface models for adhesion; (c) effective adhesion models (e.g. for peeling).

is characterized by constitutive laws relating kinematic quantities – like displacements or strains – to kinetic quantities – likes forces or stresses. In principle, an interface model is also required for case (a) in order to describe the behavior at interfaces $\mathcal{B}_1$-$\mathcal{B}_i$ and $\mathcal{B}_i$-$\mathcal{B}_2$. But for this, full bonding may simply be assumed. On the other hand, interface models can also be obtained from the projection of material models onto a surface – e.g. the interface between adherent and adhesive. This is discussed further in Sec. 3.5.4. Effective adhesion models are essentially a result of the local material and interface behavior, and they can be derived as such, see Sec. 4. Dry adhesion (i.e. adhesiveless adhesion) – like van der Waals adhesion, electrostatic attraction, or mechanical interlocking – are natural candidates for interface models. Adhesive-based adhesion – e.g. based on polymeric adhesives or capillary adhesion – are natural candidates for material models.

Before discussing the different adhesion models, we provide a very brief overview of the governing equations of continuum mechanics and their finite element discretization. Further details can for example be found in Holzapfel (2000); Wriggers (2008). A mechanical body $\mathcal{B}$ has to satisfy the equilibrium equation

$$\operatorname{div} \boldsymbol{\sigma} + \boldsymbol{f} = \rho\, \boldsymbol{a} \tag{1}$$

at all $\boldsymbol{x} \in \mathcal{B}$ along with the boundary conditions

$$\begin{aligned} \boldsymbol{u} &= \bar{\boldsymbol{u}} \quad \text{on } \partial_u \mathcal{B}\,, \\ \boldsymbol{t} &= \bar{\boldsymbol{t}} \quad \text{on } \partial_t \mathcal{B}\,, \end{aligned} \tag{2}$$

where $\partial_u \mathcal{B}$ and $\partial_t \mathcal{B}$ are the boundaries where displacements and tractions are prescribed. Here, $\boldsymbol{\sigma}$ denotes the (Cauchy) stress tensor inside $\mathcal{B}$, while $\boldsymbol{t} = \boldsymbol{\sigma}\boldsymbol{n}$ denotes the traction vector at

surfaces with normal vector $\boldsymbol{n}$; $\boldsymbol{f}$ denotes distributed body forces, while ρ and $\boldsymbol{a}$ denote density and acceleration. The latter is only needed within a dynamic analysis. In the static case, $\boldsymbol{a} = \boldsymbol{0}$. Eq. (1) is also know as the strong from of the equilibrium equation. It can be turned into the weak form statement

$$\sum_I \left[\int_{\mathcal{B}_I} \delta\boldsymbol{u} \cdot \rho\, \boldsymbol{a}\, \mathrm{d}v + \int_{\mathcal{B}_I} \operatorname{grad} \delta\boldsymbol{u} : \boldsymbol{\sigma}\, \mathrm{d}v - \int_{\mathcal{B}_I} \delta\boldsymbol{u} \cdot \boldsymbol{f}\, \mathrm{d}v - \int_{\Gamma_I} \delta\boldsymbol{u} \cdot \boldsymbol{t}\, \mathrm{d}a \right] = 0 \ , \tag{3}$$

which is valid for all functions $\delta\boldsymbol{u}$, know as virtual displacements, that are kinematically admissible. The summation is carried out over all bodies $\mathcal{B}_I$ and interfaces Γ_I in the system. The corresponding volume and surface integrals denote the virtual work done on those volumes and surfaces. In order to solve general problems in continuum mechanics – even for the linear case – computational approaches are needed. The most widely used approach is the finite element method (Zienkiewicz et al., 2005; Zienkiewicz and Taylor, 2005; Belytschko et al., 2000; Wriggers, 2008). The finite element method finds approximate solutions satisfying weak form (3). Given a discretization of the body and its surfaces into a set of elements and nodes, the displacement field $\boldsymbol{u}(\boldsymbol{x})$ is approximated by the interpolation

$$\boldsymbol{u}^h(\boldsymbol{x}) = \sum_A N_A(\boldsymbol{x})\, \boldsymbol{u}_A \ . \tag{4}$$

where $\boldsymbol{u}_A$ are the nodal displacements values, and N_A denotes the interpolation (or shape) function of node A. Standard shape functions are based on Lagrange polynomials, but in recent years also shape functions based on Bézier splines have become popular (Cottrell et al., 2009). Those can be conveniently incorporated into interpolation (4) using the Bézier extraction operator technique (Borden et al., 2011; Scott et al., 2011). The discretization of weak form (3) leads to a discretized equilibrium equation – in general non-linear – that is solved for all the unknown nodal finite element displacements $\boldsymbol{u}_A$. In the case of dynamic problems, the solution is obtained by time-stepping algorithms like Newmark's method (Wriggers, 2008).

2 Local material models for adhesives

This section surveys mechanical constitutive models that describe the material behavior within adhesives according to Fig 1a. Such models relate the stress tensor $\boldsymbol{\sigma}$ to the deformation of the material. Elasticity, viscosity, plasticity, fracture, damage, thermal effects, curing, aging and liquid bridges are discussed in the following.

2.1 Elasticity models

Elasticity describes reversible, rate-independent deformation. Corresponding models can be linear or non-linear. In linear elasticity, the stress is given by (Timoshenko and Goodier, 1970)

$$\sigma_{ij} = \mathbb{C}_{ijk\ell}\, \varepsilon_{k\ell} \tag{5}$$

where $\mathbb{C}_{ijk\ell}$ is the material tangent (a fourth order tensor) and

$$\varepsilon_{k\ell} = \frac{1}{2}\left(\frac{\partial u_k}{\partial X_\ell} + \frac{\partial u_\ell}{\partial X_k} \right) \tag{6}$$

is the strain associated with small displacements $\boldsymbol{u} = \boldsymbol{u}(\boldsymbol{X})$. The notation above uses index notation associated with Cartesian coordinates. In tensor notation the above expressions become

$$\boldsymbol{\sigma} = \mathbb{C} : \boldsymbol{\varepsilon} \ , \quad \boldsymbol{\varepsilon} = \frac{1}{2}\big(\operatorname{Grad} \boldsymbol{u} + (\operatorname{Grad} \boldsymbol{u})^T\big) \ , \quad \operatorname{Grad} \boldsymbol{u} := \frac{\partial \boldsymbol{u}}{\partial \boldsymbol{X}} \ . \tag{7}$$

In case of isotropy, $\mathbb{C}$ has the Cartesian components

$$\mathbb{C}_{ijk\ell} = \lambda\,\delta_{ij}\delta_{k\ell} + \mu\,(\delta_{ik}\delta_{j\ell} + \delta_{i\ell}\delta_{jk}) \ , \tag{8}$$

where $\lambda = \dfrac{2\mu\nu}{1-2\nu}$ and $\mu = \dfrac{E}{2(1-\nu)}$ are the bulk and shear moduli related to Young's modulus E and Poisson's ratio ν. δ_{ij} are the components of the identity tensor $\boldsymbol{I}$. It follows that

$$\boldsymbol{\sigma} = \lambda\,\mathrm{tr}\,\boldsymbol{\varepsilon}\,\boldsymbol{I} + 2\mu\,\boldsymbol{\varepsilon} \ , \tag{9}$$

or in Cartesian components

$$\sigma_{ij} = \lambda\,\varepsilon_{kk}\,\delta_{ij} + 2\mu\,\varepsilon_{ij} \ , \tag{10}$$

where $\mathrm{tr}\,\boldsymbol{\varepsilon} = \varepsilon_{kk} = \varepsilon_{11} + \varepsilon_{22} + \varepsilon_{33}$.
For general non-linear elasticity the stress tensor is given as

$$\boldsymbol{\sigma} = \boldsymbol{\sigma}(\boldsymbol{F}) \ , \tag{11}$$

where $\boldsymbol{F}$ is the deformation gradient that is related to the displacement gradient by

$$\boldsymbol{F} = \boldsymbol{I} + \mathrm{Grad}\,\boldsymbol{u} \ , \tag{12}$$

where the displacement vector $\boldsymbol{u} = \boldsymbol{x} - \boldsymbol{X}$, between deformed and undeformed structure, can now become arbitrarily large. As a further generalization the stress may also be dependent on higher deformations gradients like $\mathrm{Grad}\,\boldsymbol{F}$, a formulation known as gradient elasticity. Formulation (11) can capture both geometrical non-linearities (through $\boldsymbol{F}$) and non-linear material behavior (through the function $\boldsymbol{\sigma}(\boldsymbol{F})$) that are associated with large deformations. An important subset of non-linear elasticity is hyperelasticity. In this case, elasticity is described by the stored energy function $W = W(\boldsymbol{F})$. This setup follows from the consistency with the 2nd law of thermodynamics. The stress tensor is then defined from the derivative of W with respect to $\boldsymbol{F}$. An example is the isotropic Neo-Hookean material model (Zienkiewicz and Taylor, 2005)

$$\boldsymbol{\sigma} = \frac{\lambda}{J}\ln J\,\boldsymbol{I} + \frac{\mu}{J}\big(\boldsymbol{F}\boldsymbol{F}^T - \boldsymbol{I}\big) \ , \tag{13}$$

or in components

$$\sigma_{ij} = \frac{\lambda}{J}\ln J\,\delta_{ij} + \frac{\mu}{J}\big(F_{ik}F_{jk} - \delta_{ij}\big) \ , \tag{14}$$

where $J = \det \boldsymbol{F}$ denotes the volume change during deformation. Other examples are the Mooney-Rivlin, Ogden and Arruda-Boyce material models (Ogden, 1987; Holzapfel, 2000).
The modeling introduced above describes purely elastic behavior and does not introduce material degradation or failure. It is therefore straightforward to use in the finite element analysis of adhesively bonded joints as long as the geometry is simple and no debonding occurs. The linear, isotropic elasticity analysis of such joints goes back to the works of Anderson et al. (1973) and Adams and Peppiatt (1974). A more recent example is the work of Wu and Crocombe (1996). An important aspect of elasticity is the emergence of stress singularities at corners and material interfaces. Such singularities are for example studied in the work of Destuynder et al. (1992) or recently by Zhao et al. (2011b,a). It is also possible to consider linear elasticity of the material but account for geometrical non-linearites due to large deformations. Examples of this approach include Crocombe and Adams (1981); Apalak and Engin (1997); Andruet et al. (2001). An example for fully non-linear elasticity based on the Neo-Hookean model is given by Lubowiecka et al. (2012). Adhesion problems with linear elastic material behavior can also be studied by boundary element methods, e.g. see Salgado and Aliabadi (1998).

The elastic material behavior of adhesives can also be characterized by constraints. A common example is incompressibility, where $\nu = 0.5$. Formally this constraint is written as

$$g(\boldsymbol{F}) := J - 1 = 0 \ . \tag{15}$$

Rubber-like materials often exhibit such behavior. It is not advisable to use the models described above with simply setting $\nu \to 0.5$ due to the numerical ill-conditioning that follows as $\lambda \to \infty$. Special material models – along with corresponding computational formulations – have been developed for incompressibility. An example is the incompressible Neo-Hookean material model

$$\boldsymbol{\sigma}(\boldsymbol{F}, p) = \mu \, \boldsymbol{F}\boldsymbol{F}^T - p \, \boldsymbol{I} \ , \tag{16}$$

where p is the hydrostatic pressure field associated with constraint (15). This pressure is now independent of the deformation and thus needs to be included as an unknown within the numerical formulation. It then follows from the equilibrium equations and boundary conditions (Holzapfel, 2000).
Even though elastic material behavior is rate-independent, it can still be used within a dynamic analysis. In that case, the moving material also contributes inertial forces that are proportional to the material density and acceleration, and need to be accounted for in Eq. (1). Purely elastic materials are energy conserving and do not dissipate any energy over time. In order to account for material dissipation, viscosity or plasticity models are needed.

2.2 Viscosity and visco-elasiticity models

Viscosity is a major property of fluids. Visco-elasticity describes rate-dependent, delayed elasticity. Both can be described by simple rheological models combining elastic springs and viscous dash-pots that are shown in Fig. 2. The Maxwell element describes fluid-like behavior. The

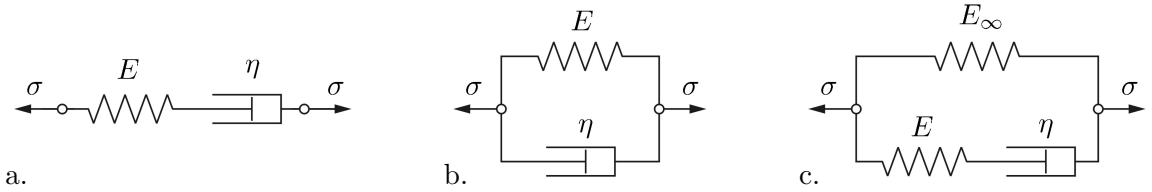

Figure 2: Viscous material models: (a) Maxwell element; (b) Kelvin element; (c) Generalized Solid.

deformation is composed of the elastic deformation in the spring and the inelastic deformation in the dash-pot, i.e.

$$\varepsilon = \varepsilon_{\text{el}} + \varepsilon_{\text{in}} \ . \tag{17}$$

The stress in spring and dash-pot is equal and given as

$$\sigma = E \, \varepsilon_{\text{el}} = \eta \, \dot{\varepsilon}_{\text{in}} \ . \tag{18}$$

The Kelvin element describes solid-like behavior. Here the strain is equal,

$$\varepsilon = \varepsilon_{\text{el}} = \varepsilon_{\text{in}} \ , \tag{19}$$

while the stresses are added,

$$\sigma = E \, \varepsilon_{\text{el}} + \eta \, \dot{\varepsilon}_{\text{in}} \ . \tag{20}$$

For a further discussion of these models and combination of them see for example Holzapfel (2000) and Sancaktar (2011). These models can also be extended to 3D by replacing the 1D stress and strain by their 3D tensorial counterparts. The elastic part can then be modeled by any of the models discussed in the preceding section. A popular model for 3D viscosity is a Newtonian fluid given by

$$\boldsymbol{\sigma} = 2\eta\, \boldsymbol{D} \ , \tag{21}$$

where

$$\boldsymbol{D} = \frac{1}{2}\big(\operatorname{grad} \boldsymbol{v} + (\operatorname{grad} \boldsymbol{v})^T\big) \ , \quad \operatorname{grad} \boldsymbol{v} := \frac{\partial \boldsymbol{v}}{\partial \boldsymbol{x}} \ , \tag{22}$$

is the symmetrized velocity gradient.
An important combination is the generalized solid model, where a spring is considered in parallel to one (or several) Maxwell elements (see Fig. 2c). The single spring describes the elastic response at (thermodynamic) equilibrium, while the Maxwell element(s) describes non-equilibrated states. Like in the Kelvin element the corresponding stresses are added,

$$\boldsymbol{\sigma} = \boldsymbol{\sigma}_{\mathrm{eq}} + \boldsymbol{\sigma}_{\mathrm{neq}} \ , \tag{23}$$

while the strains, equal in all parallel elements, are added within each Maxwell element,

$$\boldsymbol{\varepsilon} = \boldsymbol{\varepsilon}_{\mathrm{el}} + \boldsymbol{\varepsilon}_{\mathrm{in}} \ . \tag{24}$$

In the 1D setting we have $\sigma_{\mathrm{eq}} = E_\infty\, \varepsilon$ and $\sigma_{\mathrm{neq}} = E\, \varepsilon_{\mathrm{el}} = \eta\, \dot{\varepsilon}_{\mathrm{in}}$. The formulation can be extended to the non-linear setting considering both non-linear behavior of the elastic and viscous parts. Instead of the additive decomposition (24), it is then customary to consider a multiplicative decomposition of the deformation gradient, as

$$\boldsymbol{F} = \boldsymbol{F}_{\mathrm{el}}\, \boldsymbol{F}_{\mathrm{in}} \ . \tag{25}$$

The inelastic strains ($\boldsymbol{\varepsilon}_{\mathrm{in}}$ or $\boldsymbol{F}_{\mathrm{in}}$) are viewed as internal variables, which track microstructural changes in the material that are not observable from the outside. An additional law is needed to describe the evolution of these internal variables. For further details see Holzapfel (2000).
It is noted that viscosity is usually temperature dependant, e.g. see (Sancaktar, 2011). It is also noted that viscosity leads to energy dissipation in the system. However, the presence of dissipation in the system does not imply that the adhesive is dissipative. Dissipation can also occur in the adherents. Further properties of viscous materials are also discussed in Dillard (2011).
The three-parameter linear visco-elasticity model of Fig. 2.c has been applied to study joints by Yadagiri et al. (1987). The linear visco-elastic Kelvin model has been used to study bonded connections by Carpenter (1990). A Newtonian fluid model has been used in Lin et al. (2002) to model fibril behavior in debonding. Simple linear visco-elasticity models for the adherents have also been used in combination with van der Waals interaction to study gecko adhesion by Sauer (2010) and Tang and Soh (2011). It seems, that so far the use of non-linear viscous and visco-elastic models has not been applied to adhesion.

2.3 Plasticity and damage models

Plasticity and damage describe irreversible changes during deformation. Rheologically this can be described by slider elements that open up once the stress reaches a limit value σ_{y}, the so called yield stress. Examples are shown in Fig. 3. Mathematically, the two cases are described by

$$\varepsilon = \varepsilon_{\mathrm{el}} + \varepsilon_{\mathrm{in}} \ , \tag{26}$$

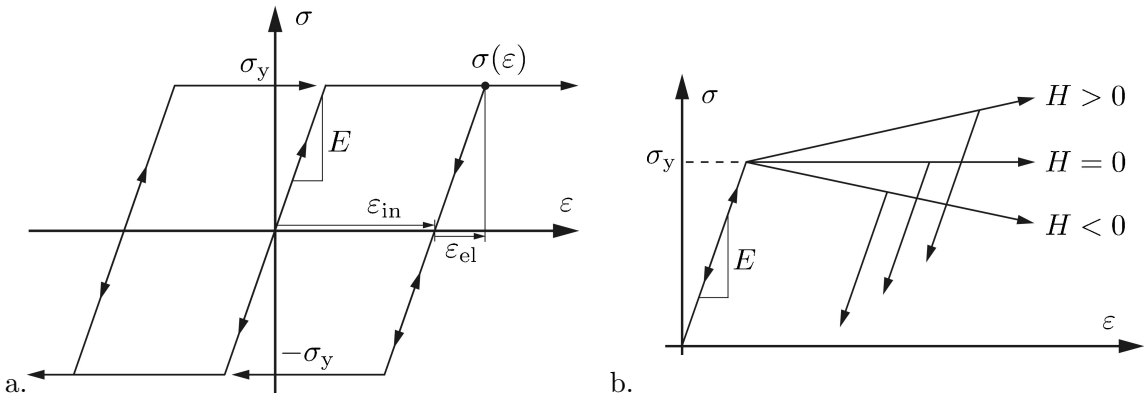

Figure 3: Plasticity models: (a) plastic loading and unloading; (b) linear hardening and softening.

and

$$\sigma = E\,\varepsilon_{\mathrm{el}}\ , \quad \sigma \leq \sigma_{\mathrm{y}} + H\,\varepsilon_{\mathrm{in}}\ , \tag{27}$$

where now $\varepsilon_{\mathrm{in}}$ denote the plastic strains that remain in the material after unloading, and where H models hardening during plastic deformation. $H = 0$ corresponds to the behavior in Fig. 3a. The limit equation on σ is also know as the yield criterion. A typical example in 3D is the von Mises yield criterion (Simo and Hughes, 1998)

$$f := \|\boldsymbol{s}\| - \sqrt{\tfrac{2}{3}}\,\sigma_{\mathrm{y}} \leq 0\ , \tag{28}$$

where $\boldsymbol{s}$ is the deviatoric part of the stress tensor $\boldsymbol{\sigma}$ and $\|\boldsymbol{s}\| := \sqrt{\boldsymbol{s} : \boldsymbol{s}}$ denotes the tensor norm. Based on this, the distinction

$$\begin{aligned} f < 0 \quad & \text{elastic state} \\ f = 0 \quad & \text{plastic state} \end{aligned} \tag{29}$$

is made. In the non-linear setting, the additive strain decomposition is usually replaced by a multiplicative split as in Eq. (25).

In this framework, also damage can be modeled, considering material softening (for $H < 0$) due to material degradation. Such a process is often driven by cyclic loading (i.e. fatigue). Alternatively, damage can also be modeled by local fracture, as is discussed in the following section. A further overview of rheological damage models for adhesives is given in Sancaktar (2011). An overview of general computational approaches is given in Simo and Hughes (1998). Linear elasto-plastic adhesive behavior is considered in Edlund and Klarbring (1990). In that work the deformation behavior of the adhesive is simplified such that it can be treated computationally as a flat interface (in a similar manner as contact). The work is later extended to non-linear elasticity (Edlund and Klarbring, 1992) and to account for damage (Edlund and Klarbring, 1993; Edlund, 1994; Schmidt and Edlund, 2006). The last reference is based on the asymptotic expansion technique of Klarbring (1991) and Klarbring and Movchan (1998). In later work, also visco-plasticity is considered as a numerical regularization technique (Schmidt and Edlund, 2010). In Cui et al. (2003) the authors consider von-Mises plasticity to model adhesive failure during peeling. Plasticity can also be considered in the context of interface models, see Sec. 3.3 below. An example is the work of Créac'hcadec et al. (2008) and Créac'hcadec and Cognard (2009).

2.4 Fracture models

Fracture mechanics describes local material damage and failure due to the appearance of cracks. Cracks imply that new surfaces are created and the topology of the body thus changes. The fracturing process can be brittle or ductile. Cracks can appear in the adhesive and adherents, or between the two. In the latter case one speaks of debonding between adhesive and adherent, which can also be treated by interface models (see Sec. 3). In the following, the two most common computational finite element (FE) approaches to fracture are described briefly. Those are cohesive zone models (CZM) and extended finite element methods (XFEM). CZM introduce interface laws between elements that allow for possible separation of the elements. They are fairly easy to implement, but introduce a FE mesh dependency of the crack path. They are therefore ideal for failure along a predefined crack path, e.g. for failure along a known interface. CZM are therefore commonly used in the context of interface models, discussed in detail in the following section (see Sec. 3). An application of CZM to study fracture within the adhesive layer is considered by Martiny et al. (2008).
XFEM circumvent the problem of mesh dependency, but they are much more difficult to implement, especially in 3D. The basic idea is to enrich the numerical solution at the crack tip, for example with the solutions known from analytical fracture mechanics. Interpolation (4) then takes the form

$$\boldsymbol{u}^h(\boldsymbol{x}) = \sum_A N_A(\boldsymbol{x})\,\boldsymbol{u}_A + \sum_A \hat{N}_A(\boldsymbol{x})\,\psi(\boldsymbol{x})\,\boldsymbol{q}_A \ , \tag{30}$$

where $\hat{N}_A$ are standard FE shape functions, possibly identical to N_A, $\psi(\boldsymbol{x})$ is the enrichment, and $\boldsymbol{q}_A$ are additional nodal unknows associated with the enrichment. The approach goes back to Moës et al. (1999). An overview of further developments is reported in Belytschko et al. (2009) and Fries and Belytschko (2010). An application to the failure of adhesives is considered in Campilho et al. (2011).

2.5 Thermo-mechanical models

Thermo-mechanical models describe the coupling between thermal and mechanical behavior, i.e. they capture the dependence of deformation (and stress) on temperature, and the dependence of temperature on deformation and stress. To capture those, the mechanical equilibrium equations need to be coupled with the energy balance (the first law of thermodynamics). Further, the mechanical material models describing elasticity, viscosity and plasticity become temperature dependent in general, while the thermal material model describing conductivity becomes deformation dependent. The framework of such models is discussed by Holzapfel (2000) in the general context of large deformations. A simplified approach is to disregard the influence of deformation on temperature and to account for additive thermal strains due to the temperature increase ΔT as

$$\boldsymbol{\varepsilon} = \boldsymbol{\varepsilon}_{\mathrm{el}} + \boldsymbol{\varepsilon}_{\mathrm{temp}} \ , \quad \boldsymbol{\varepsilon}_{\mathrm{temp}} = \alpha_{\mathrm{T}}\,\Delta T\,\boldsymbol{I} \ , \tag{31}$$

where α_{T} is the thermal coefficient of expansion. For linear elasticity, the resulting stresses then follow from Hooke's law, $\boldsymbol{\sigma} = \mathbb{C} : \boldsymbol{\varepsilon}_{\mathrm{el}}$. In the nonlinear setting the additive strain decomposition should again be replaced by a multiplicative split, e.g. in the form

$$\boldsymbol{F} = \boldsymbol{F}_{\mathrm{el}}\,\boldsymbol{F}_{\mathrm{temp}} \ , \quad \boldsymbol{F}_{\mathrm{temp}} = (1 + \alpha_{\mathrm{T}}\,\Delta T)\,\boldsymbol{I} \ . \tag{32}$$

The elastic stresses then follow from a model like Eq. (13) using $\boldsymbol{F}_{\mathrm{el}}$ as the functional argument. Like in the linear case, this model does not account for the full thermo-mechanical coupling. Some of the thermal properties of adhesives are discussed in Comyn (2011). Computational examples of thermo-mechanical analysis of adhesive joints can be found in He (2011).

2.6 Curing models

Curing describes the chemical cross-linking of polymer chains. These chains form the chemical structure of most industrial adhesives. For rubbers, the curing process is usually referred to as vulcanization. Curing is often facilitated by heat, UV light, or chemical additives. It leads to a change of the material properties of the adhesive, usually transforming the adhesive from a viscous liquid into a visco-elastic solid. During curing, thermal expansion and in particular chemical shrinkage[4] of the material can occur, leading to residual stress states. Corresponding models have been considered by White and Hahn (1992) and Adolf and Martin (1996). Thermodynamically derived computational curing models for finite deformations have been formulated recently by Lion and Höfer (2007) and Hossain et al. (2009, 2010). The modeling has also been extended to account for the damage due to curing shrinkage (Mergheim et al., 2012). A computational formulation that aims to model rubber vulcanization and its coupling with thermo-mechanics is given in André and Wriggers (2005). A challenge in formulating general non-linear material models is the experimental difficulty to properly characterize the full range of the material behavior. This calls for more experiments. A recent overview of some experimental curing data is provided in Comyn (2011), Sancaktar (2011) and Yu et al. (2013).

2.7 Ageing models

Ageing describes the change – usually degradation – of material properties over time, and it thus affects the durability of adhesive bonds. Like curing, ageing is often affected by temperature, humidity, light or chemical agents. Strong and stiff materials can thus become weak and soft over time. In the case of adhesives, the cross-linking of polymer chains can decrease so much that the material becomes soft, perhaps even liquid. On the other hand, the cross-linking can also increase over time, e.g. due to long-term UV light exposure, making the material too brittle. The effect of ageing on the mechanics of adhesive joints due to moisture is considered in the FE studies of Loh et al. (2003) and Liljedahl et al. (2005). Further works can be found in the review by He (2011). An overview of the modeling of moisture diffusion into adhesives and its effect on adhesive joints is discussed in Ashcroft and Comyn (2011), Comyn (2013), Ashcroft and Crocombe (2013) and Crocombe and Ashcroft (2013). Diffusion is commonly described by Fick's laws (Comyn, 2013). In general, diffusion and deformation can be fully coupled such that diffusion depends on deformation and deformation depends on diffusion. In this case one has to combine the equilibrium Eq. (1) with the advection-diffusion equation stemming from mass balance. Like for curing, a challenge in the modeling of ageing is the experimental complexity required to assess the full range of general non-linear material models. On the other hand, an advantage in the modeling of ageing is the temporal scale separation between mechanical motion and ageing: The former usually varies much faster than the latter, allowing to decouple the two processes.
Related to ageing is the phenomenon of fatigue due to cyclic loading. Various models exist in the context of fatigue to describe the ensuing material degradation (Suresh, 1998). The influence of fatigue on adhesive joints is discussed in Ashcroft (2011) and Crocombe and Ashcroft (2013). Fatigue induces microscopic damage that can be modeled according to Sec. 2.3.

[4] A simple model for shrinkage and swelling due to concentrational changes Δc, is given by model (31), or (32) respectively, when ΔT is replaced by Δc. α_{T} then plays the role of the swelling coefficient.

2.8 Capillary adhesion models

Liquids form menisci that exert capillary forces at interfaces. An example is a liquid bridge between two solids. The capillary forces of the liquid bridge provide adhesion between the solids. The surface tension of the capillary bridge effectively pulls the two bodies together. In the following, we discuss explicit models for liquid bridges; effective interface models due to liquid bridges are discussed in Sec. 4 below. Liquid bridges can be modeled explicitly based on the membrane equations governing the surface shape of the liquid bridge. In case of liquids with constant, isotropic surface tension the surface shape is governed by the Young-Laplace equation

$$2H\gamma + p = 0 \ , \tag{33}$$

where $2H$ is the mean curvature of the surface and p is the pressure difference across the surface. A contact angle forms at the contact line where the liquid bridge connects with the solid. This angle is governed by the surface tensions of the three interfaces: liquid-gas, liquid-solid and solid-gas. If the solid is soft, a wetting ridge can be observed at the contact line (Sauer, 2014b). For liquid bridges, the Young-Laplace equation replaces equilibrium equation (1).
The analytical solution of (33) for axisymmetric liquid bridges for negligible gravity (i.e. constant p) is provided by Orr et al. (1975). Numerical integration of (33) for axisymmetric menisci is discussed for example in Padday (1971). More general cases can be analyzed by finite element methods (Brown et al., 1980) and energy minimization methods (Brakke, 1992; Iliev, 1995). In Sauer (2014c) a new and very general finite element formulation is developed for liquid films, in order to analyze capillary forces. An example is shown in Fig. 4. At small length scales, the

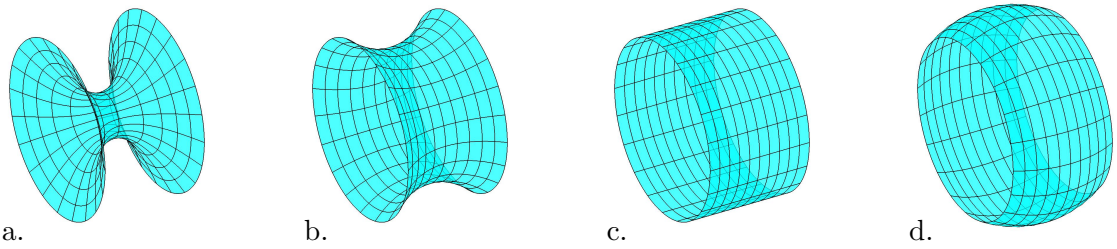

Figure 4: Finite element analysis of a liquid bridge for different contact angles (Sauer, 2014c)

relative humidity has a strong influence on capillary forces (Pakarinen et al., 2005). A recent survey of capillary forces between flat and spherical surfaces – accounting also for the viscous forces from the fluid flow – is given by Cai and Bhushan (2008).

3 Local interface models for adhesion

This section surveys mechanical constitutive models that describe the interface behavior between adherents according to Fig 1b. Such models relate the interface traction $\boldsymbol{t}$ to the separation of the two surfaces.

Interface adhesion is closely related to interface contact. In some sense adhesion corresponds to 'the other side of contact' – describing the interaction of solids as they are pulled apart instead of pushed together. A survey of contact formulations and corresponding computational models has been provided recently by Zmitrowicz (2010). Comprehensive background information on

computational contact formulations can be found in the monographs of Laursen (2002) and Wriggers (2006).

3.1 Theoretical description of local interface interactions

In a general sense all mechanical interface models can be associated with traction-separation laws that relate the local interface traction $\boldsymbol{t}$ to the pointwise surface separation $\boldsymbol{g}$, also referred to as the gap vector or displacement jump. According to Fig. 5, the surface separation of point

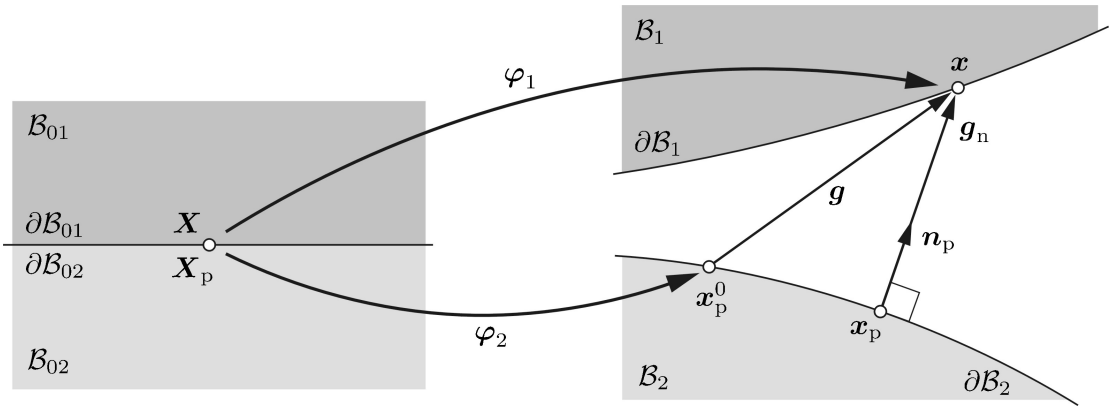

Figure 5: Separation kinematics: Definition of the gap vectors $\boldsymbol{g}$ and $\boldsymbol{g}_\mathrm{n}$ between surfaces $\partial\mathcal{B}_1$ and $\partial\mathcal{B}_2$ at point $\boldsymbol{x} \in \partial\mathcal{B}_1$ that is initially located at $\boldsymbol{X} \in \partial\mathcal{B}_{01}$.

$\boldsymbol{X}$ can be defined as

$$\boldsymbol{g}(\boldsymbol{X}) = \boldsymbol{x} - \boldsymbol{x}_\mathrm{p}^0 \ , \tag{34}$$

with

$$\boldsymbol{x} = \boldsymbol{\varphi}_1(\boldsymbol{X}) \ , \quad \boldsymbol{x}_\mathrm{p}^0 = \boldsymbol{\varphi}_2(\boldsymbol{X}_\mathrm{p}) \ . \tag{35}$$

Here $\boldsymbol{\varphi}_1$ and $\boldsymbol{\varphi}_2$ denote the deformation maps between undeformed and deformed surface configurations, and $\boldsymbol{X}_\mathrm{p}$ denotes the neighbor to $\boldsymbol{X}$ in the undeformed configuration. Thus $\boldsymbol{x}_\mathrm{p}^0$ is the current location of the initial interaction point $\boldsymbol{X}_\mathrm{p}$. In general, $\boldsymbol{X}_\mathrm{p}$ is computed from a closest point projection of $\boldsymbol{X}$ onto the neighboring surface, e.g. see Wriggers (2006). In the same way, the point $\boldsymbol{x}_\mathrm{p}$ can be obtained from $\boldsymbol{x}$. Some traction-separation laws are formulated in terms of the normal gap

$$\boldsymbol{g}_\mathrm{n}(\boldsymbol{X}) = \boldsymbol{x} - \boldsymbol{x}_\mathrm{p} \ , \tag{36}$$

i.e. the interaction takes place between $\boldsymbol{x}$ and $\boldsymbol{x}_\mathrm{p}$, and not between $\boldsymbol{x}$ and $\boldsymbol{x}_\mathrm{p}^0$. An example is van der Waals adhesion (see below).
A simple traction-separation law is the tri-linear model (Tvergaard and Hutchinson, 1992)

$$\boldsymbol{t}(\boldsymbol{g}) = -\,\bar{\boldsymbol{g}} \times \begin{cases} t_0 \dfrac{g}{g_0} & \text{if } 0 \le g < g_0 \ , \\ t_0 & \text{if } g_0 \le g \le g_1 \ , \\ t_0 \dfrac{g - g_2}{g_1 - g_2} & \text{if } g_1 < g < g_2 \ , \\ 0 & \text{if } g_2 \le g \ . \end{cases} \tag{37}$$

Here $\bar{\boldsymbol{g}} := \boldsymbol{g}/\|\boldsymbol{g}\|$ denotes the direction and $g := \|\boldsymbol{g}\|$ the magnitude of $\boldsymbol{g}$, while t_0, g_1 and g_2 are model parameters. A visualization of (37) is shown in Fig. 6a. Special cases are obtained for $g_0 = 0$ and/or $g_1 = g_0$. The model is both suitable for normal and tangential debonding.

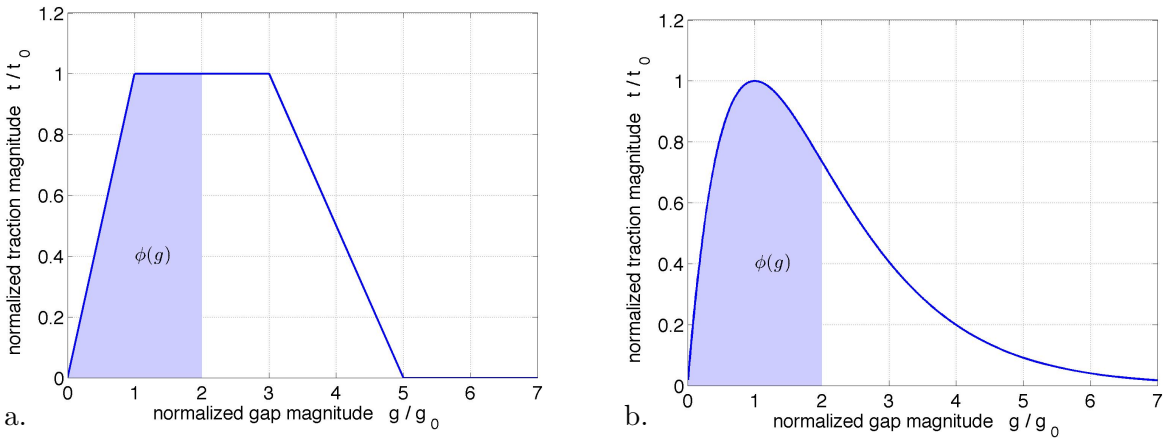

Figure 6: Traction-separation models: (a) Tri-linear model (37) for $g_1 = 3g_0$ and $g_2 = 5g_0$; (b) Exponential model (38). $\phi(g)$ denotes the separation energy up to g ($= 2g_0$, here).

It is also possible to formulate separate laws (with separate parameters) for the normal and tangential components of the traction. Such an approach can be useful in order to distinguish between normal and tangential debonding behavior.
If the gap closes, contact can occur. In that case, law (37) is not suitable anymore and should be replaced by contact and friction models. The kinematical framework presented above is also suitable to describe contact, so that CZM and contact models can be combined. Therefore it is helpful to formulate contact by allowing a penetration to occur. This is the case when $\boldsymbol{g}_\mathrm{n} \cdot \boldsymbol{n}_\mathrm{p} < 0$, where $\boldsymbol{n}_\mathrm{p}$ is the outward surface normal at $\boldsymbol{x}_\mathrm{p}$ (see Fig. 5).
Another example is the exponential model

$$\boldsymbol{t}(\boldsymbol{g}) = -\frac{t_0}{g_0} \exp\left(1 - \frac{g}{g_0}\right) \boldsymbol{g} \ , \tag{38}$$

which is a special case of the cohesive zone model of Xu and Needleman (1993). A visualization of (38) is shown in Fig. 6b. A clear advantage of (38) over (37) is that it is differentiable for all values of g.
A third example is the traction-separation law for van der Waals adhesion,

$$\boldsymbol{t}(\boldsymbol{g}_\mathrm{n}) = \frac{A_\mathrm{H}}{2\pi g_0^3}\left[\frac{1}{45}\left(\frac{g_0}{g_\mathrm{n}}\right)^9 - \frac{1}{3}\left(\frac{g_0}{g_\mathrm{n}}\right)^3\right] \boldsymbol{n}_\mathrm{p} \ , \quad \text{for } g_\mathrm{n} := \|\boldsymbol{g}_\mathrm{n}\| > 0 \ , \tag{39}$$

were g_0 denotes the atomic equilibrium spacing and A_H denotes Hamaker's constant. Qualitatively, law (39) looks like law (38) shown in Fig. 6b. Eq. (39) is obtained from analytical integration of the Lennard-Jones potential over body $\mathcal{B}_2$, e.g. see Sauer and Wriggers (2009). This integration is based on certain assumptions on the deformation (see also Sec. 3.5.2) that may not be satisfied in general. In general, numerical integration of the Lennard-Jones potential needs be considered (Sauer and Li, 2007b).
All the laws specified above can be derived from a potential ϕ. The values $\phi(g)$ and $\phi(g_\mathrm{n})$ denote the separation work (per unit surface area) up to distances g and g_n. They correspond to the area beneath the traction-separation curve as shown in Fig. 6. The total area under the curves (up to $g = g_\mathrm{n} = \infty$) then corresponds to the specific *work of adhesion* (or cohesion, respectively), denoted w_adh.
There are only few cases that can be treated by analytical solution techniques – then typically in the framework of linear fracture mechanics (Gross and Seelig, 2006). In the general case, the setup is too complex to solve analytically – often due to nonlinearities arising from the geometry

(like the kinematics in Fig. 5) or the material behavior of the bulk (see Sec. 2) and interface (as in Eqs. (37)–(39)) – such that computational solution techniques are needed. The most widely used techniques are finite element methods based on Eq. (3). However, traction-separation laws can also be used in the context of boundary element methods (Nesemann and Stephan, 2012). The last two examples, Eqs. (38) and (39), show that traction-separation models can also account for long-range interaction as g becomes large. Other such examples are electrostatic and gravitational interactions, which can be cast into same framework (Sauer and De Lorenzis, 2013). The case of long-range interactions is not trivial, since the interaction kinematics illustrated in Fig. 5 can become tricky to evaluate in this case. Sauer and De Lorenzis (2013) also report a general finite element formulation for the presented interface models.

It is important to note that the debonding and the bonding process can be inherently unstable (Yao and Gao, 2006; Sauer, 2006, 2011a). The process is known as jump-off-contact and jump-to-contact. It can be illustrated from the simple model system shown in Fig. 7a. Here ϕ

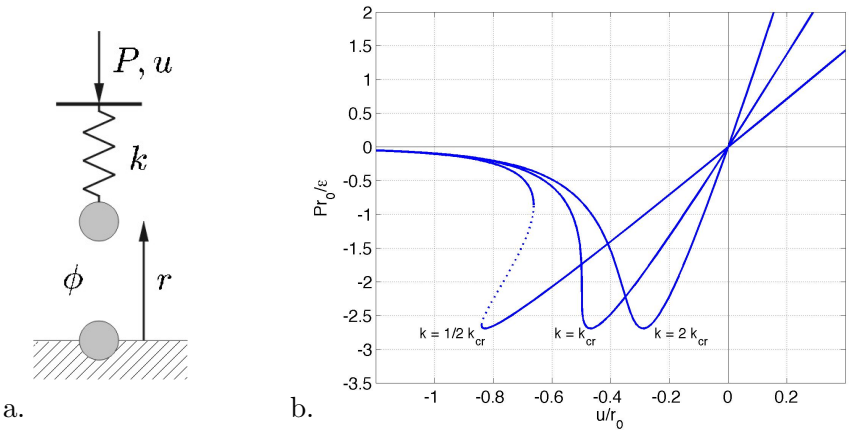

Figure 7: Debonding instability (Sauer, 2006, 2011a): (a) 1D model system, (b) resulting debonding behavior, which becomes unstable for $k < k_{\mathrm{cr}}$ (dashed line).

represents the bonding potential and k the stiffness of the adherents and their support. If k falls below a critical value k_{cr} the bonding potential overpowers the support, leading to an unstable load displacement curve $P(u)$. During a loading cycle, a hysteresis then appears, and the energy enclosed by the loading cycle is usually dissipated. Due to surface roughness many such jumps can occur (Guduru, 2007; Kesari and Lew, 2011).

Even when there is no physical instability present, the corresponding computational formulation can still become unstable if the finite element discretization is too coarse (Crisfield and Alfano, 2002; Sauer, 2011b). Essentially, the FE discretization needs to be sufficiently fine in order to capture the separation law properly. An efficient way to achieve this, is to enrich the surface discretization such as is considered by Crisfield and Alfano (2002); Guiamatsia et al. (2009); Samimi et al. (2009); Sauer (2011b, 2013); Corbett and Sauer (2014, 2015); Stapleton et al. (2014).

It is useful to classify interface models according to the following four sections:

3.2 Treatment of adherents

The mechanical behavior of the adherent surfaces can be modeled by a range of different approaches. They can be considered rigid, as elastic foundations (Johnson, 1985), elastic half-

spaces (Johnson, 1985), linear continua (Timoshenko and Goodier, 1970), or general, non-linear continua (Holzapfel, 2000) that are characterized by the material behavior outlined in Sec. 2. In principle they can also be modeled by atomistic approaches. In this case the interface interactions are governed by molecular bonds. Instead of surface tractions, we now have interaction forces acting on the individual surface atoms. Examples are given in Landman et al. (1990); Yongsheng et al. (1999); Yong et al. (2004); Luan and Robbins (2006); Yang et al. (2006); Gilabert et al. (2007); Sauer and Li (2008); Peri and Cetinkaya (2009) and Schmidt et al. (2014). Another aspect is the surface roughness. How it is accounted for? As an effective roughness parameter – like the root mean square roughness (Persson et al., 2005) – or explicitly, as for example in the simulations of Sauer and Holl (2013)?

3.3 Reversibility of interactions

What happens when the loading is reversed and the surfaces approach each other? Do we follow the same path as during loading (shown in Fig. 6), or is there a different path for unloading? If unloading follows the same path as loading, then the model is reversible and no energy is lost during cyclic loading. Consequently the traction-separation law can be derived from a potential. An example is the Lennard-Jones potential commonly used for van der Waals interactions. If unloading follows a different path, i.e. if the debonding is irreversible, energy is dissipated and associated with a degradation of the interface bonding. The setting is analogous to the damage modeling considered in the bulk, see Sec. 2.3 and Fig. 3a. Irreversible traction-separation models have been considered by Camacho and Ortiz (1996); Ortiz and Pandolfi (1999); Raous et al. (1999); Roe and Siegmund (2003); Feng et al. (2009); Del Piero and Raous (2010); Schmidt and Edlund (2010), among others. As the gap g approaches zero (and in some models even becomes negative), classical contact – with compressive traction – occurs. In order to handle this case, a contact formulation is required, e.g. such as discussed by Laursen (2002) and Wriggers (2006).

3.4 Static vs. transient interface models

The debonding behavior may be static or dynamic. But even dynamic debonding behavior may only be an effect of the transient behavior of the adherents rather than any transient behavior of the interface model, such that in this case static bonding models of the form $\boldsymbol{t} = \boldsymbol{t}(\boldsymbol{g})$ are sufficient. On the other hand, many adhesives are visco-elastic polymers that show time-dependent and thus dissipative behavior. The traction-separation law then takes the form $\boldsymbol{t} = \boldsymbol{t}(\boldsymbol{g}, \dot{\boldsymbol{g}})$. Such models can be constructed by extending the models described above similarly to the extension considered for bulk materials (see Sec. 2.2). A formulation for time-dependent debonding has been provided by Fremond (1988), see also Sec. 3.5.1. A corresponding computational formulation is given by Raous et al. (1999). Another approach is the viscoelastic debonding law by Elmukashfi and Kroon (2014) that is based on the Kelvin element (see Fig. 2b). For a full dynamic analysis of time-dependent adhesion, also inertia needs to be accounted for. Inertia is usually only a property of the bulk material and not of the interface, as the interface is massless. Bulk inertia is accounted for in Eq. (1). However, if the interface replaces a (thin) layer of adhesive, it contributes inertia that should also be accounted for – either in Eq. (1) or by considering an interface model of the form $\boldsymbol{t} = \boldsymbol{t}(\boldsymbol{g}, \dot{\boldsymbol{g}}, \boldsymbol{a})$.

3.5 Origin of interactions

The interaction laws can have various origins. In the following we distinguish between five different cases. These are related to the way interface laws can be determined. There are two

basic approaches for this: top-down approaches based on experiments – discussed in Sec. 3.5.1 – and bottom-up approaches based on underlying mechanisms – discussed in Secs. 3.5.2–3.5.5.

3.5.1 Phenomenological traction-separation laws

Phenomenological traction-separation laws are laws that are usually determined from macro scale debonding experiments. Such laws are widely used. They are prominently known as cohesive zone models (CZM), see e.g. Tvergaard (1990); Tvergaard and Hutchinson (1992); Xu and Needleman (1993); Camacho and Ortiz (1996); van den Bosch et al. (2006). But they are sometimes also referred to as *bond-slip models*, e.g. see Eligehausen et al. (1983) and references thereof. There is also a recent review article on cohesive zone models (Liu and Zheng, 2010). CZM are mostly used for debonding, but they can also describe bonding (see Sec. 3.3). The experimental determination of cohesive zone parameters for adhesives is for example considered in Sørensen (2002); Andersson and Stigh (2004); Andersson and Biel (2006); Leffler et al. (2007); Ouyang and Li (2009); Ji et al. (2011); de Moura et al. (2012); Fernandes et al. (2013). In experiments, the loading rate can have a strong effect on the results. This implies that dissipation is present in the bulk (i.e. due to mechanisms described in Sec. 2.2–2.4) and/or in the interface (addressed in Sec. 3.3). In order to match computational results with experimental results, so-called *inverse methods* can be used. Those solve Eqns. (1)-(3) for the unknown material parameters given the deformation.

Phenomenological traction-separation laws have been considered in a huge range of different applications. For example, to simulate and study blood clotting (Fogelson, 1984), fiber debonding (Tvergaard, 1990), fracture mechanics (Tvergaard and Hutchinson, 1992; Camacho and Ortiz, 1996; Ortiz and Pandolfi, 1999), elasto-plastic peeling (Wei and Hutchinson, 1998; Yang et al., 1999), sandwich beams (Kaziolas et al., 2000), debonding of visco-elastic polymers (Rahulkumar et al., 2000), mixed-mode delamination (Borg et al., 2002), rate dependent peeling (Lin et al., 2002), interface fracture (Roe and Siegmund, 2003), coupled adhesion and friction (Talon and Curnier, 2003), adhesive contact between elasto-plastic solids (Li and Yu, 2004), elasto-plastic debonding (Su et al., 2004), dynamic thin film delamination (Hendrickx et al., 2005; Tran et al., 2008), focal cell adhesion (McGarry et al., 2005), the aggregation of cells (Armstrong et al., 2006), mode I debonding of elastic bodies (Kočvara et al., 2006), mixed-mode debonding (Li et al., 2006), microcrack decohesion (Carpinteri et al., 2008), thin film buckling (Gruttmann and Pham, 2008), multiscale modeling of cohesive failure (Matous et al., 2008), powder cohesion (Luding, 2008), debonding with mixed finite elements (Lorentz, 2008), mixed-mode debonding of reinforcement sheets (De Lorenzis and Zavarise, 2008), membrane adhesion (Zhang and Wang, 2008; Zhang et al., 2009), non-associated visco-plasticity of adhesives (Créac'hcadec and Cognard, 2009), adhesive impact of spheres accounting for hysteresis (Feng et al., 2009), bond degradation due to humidity and thermal effects (Zhang et al., 2010), debonding of lap joints (Campilho et al., 2011), adhesion of surfaces covered with micro-columns (Lin and Wu, 2012), mixed-mode debonding of DCBs (double cantilever beams) (Sauer, 2013; Stapleton et al., 2014), bonding in metal forming (Bambach et al., 2014), and fibrillation in delamination (Vossen et al., 2014). Phenomenological traction-separation laws have also been applied in the context of isogeometric analysis (Verhoosel et al., 2011; Corbett and Sauer, 2014, 2015; Dimitri et al., 2014), and they have been adapted to develop new time integration methods for adhesion and debonding (Gautam and Sauer, 2013, 2014).

Another approach, introduced by Fremond (1988), is to model adhesion and debonding by the phenomenological bonding function β – a surface state variable also called *intensity of adhesion* – that is governed by a temporal ODE. The traction-separation behavior is then governed by the evolution of β and is generally time-dependent. The formulation can thus be used to

model viscous debonding. The approach can also be combined with sliding friction (Raous et al., 1999) and damage modeling (Del Piero and Raous, 2010). The adhesion formulation of Fremond (1988) has been applied to simulate and study beam and plate delamination (Point and Sacco, 1996a,b), bone-implant bonding (Rojek and Telega, 1999, 2001; Rojek et al., 2001), beam contact (Han et al., 2002), membrane adhesion (Andrews et al., 2003), adhesion of viscoelastic bodies (Chau et al., 2003; Fernández et al., 2003; Cocou et al., 2010), plate contact (Ahn, 2008) and rubber friction (Wriggers and Reinelt, 2009). The mathematical aspects of the adhesion formulation of Fremond (1988) have been pursued further in the works of Cocou and Rocca (2000); Sofonea et al. (2006b,a); Touzaline (2010), and Bonetti et al. (2008, 2009, 2012).

The distance at which the traction according to laws like (37), (38) or (39) decays to zero may be very small, so that in this case, separation is often modeled by disregarding the actual traction-separation law but accounting instead only for the (total bonding) energy change (i.e. release or storage) due to debonding and bonding, which is given by w_{adh}. The relation between phenomenological traction-separation laws and energy release is for example discussed in Diehl (2008). An overview of the related approaches in fracture mechanics can be found in Lane (2003) and Gross and Seelig (2006). In the context of adhesion, such approaches have been e.g. considered for thin film peeling (Kendall, 1975), particle adhesion (Quesnel and Rimai, 2000), membrane adhesion (Lipowsky and Seifert, 1991; Nadler and Tang, 2008; Long et al., 2010; Long and Hui, 2012) and rough surface adhesion (Carbone et al., 2009). A related approach, that also does not use the actual surface separation, but considers an adhesion potential based on phase field functions is given in Gu et al. (2014).

Fig. 8 shows a 3D example based on a phenomenological traction-separation law: The debonding between a thin strip peeled from a flat plate (Corbett and Sauer, 2015). The simulation is based on model (38). A crucial aspect is such simulations is that the FE discretization needs to be sufficiently fine in order to capture the separation law properly. Otherwise the formulation can become numerically unstable (Crisfield and Alfano, 2002; Sauer, 2011b). This comes on top of physical instabilities inherent to debonding (see above). In the present case the largest element size is as big as $25g_0$, and the simulation will fail for a standard linear interpolation (blue curve), whereas it runs through for the enriched FE technique proposed in Corbett and Sauer (2015) (red curve). The example of Fig. 8 also shows that it is not necessary to use conforming surface meshes within the interface. In a general FE implementation of traction-separation laws, arbitrary surface meshes can be considered.

3.5.2 Molecular models for adhesion

Traction-separation laws can also originate from molecular adhesion. The most popular example is van der Waals adhesion, which is typically based on the Lennard-Jones potential. The attraction between the individual molecules of neighboring bodies can sum up to significant adhesion forces between the bodies. In the continuum limit this summation becomes an integration over the two bodies. In case of the Lennard-Jones potential

$$\phi(g) = \frac{A}{g^{12}} - \frac{B}{g^6} \ , \tag{40}$$

where A and B are model parameters, this integration gives the global interaction potential

$$\Pi = \int_{\mathcal{B}_1} \int_{\mathcal{B}_2} \rho_1 \, \rho_2 \, \phi \, \mathrm{d}v_2 \, \mathrm{d}v_1 \ , \tag{41}$$

where ρ_k $(k = 1, 2)$ is the molecular density of body $\mathcal{B}_k$. This integration can be evaluated analytically – for rigid objects, like spheres (Bradley, 1932; Hamaker, 1937) and shells (Tadmor,

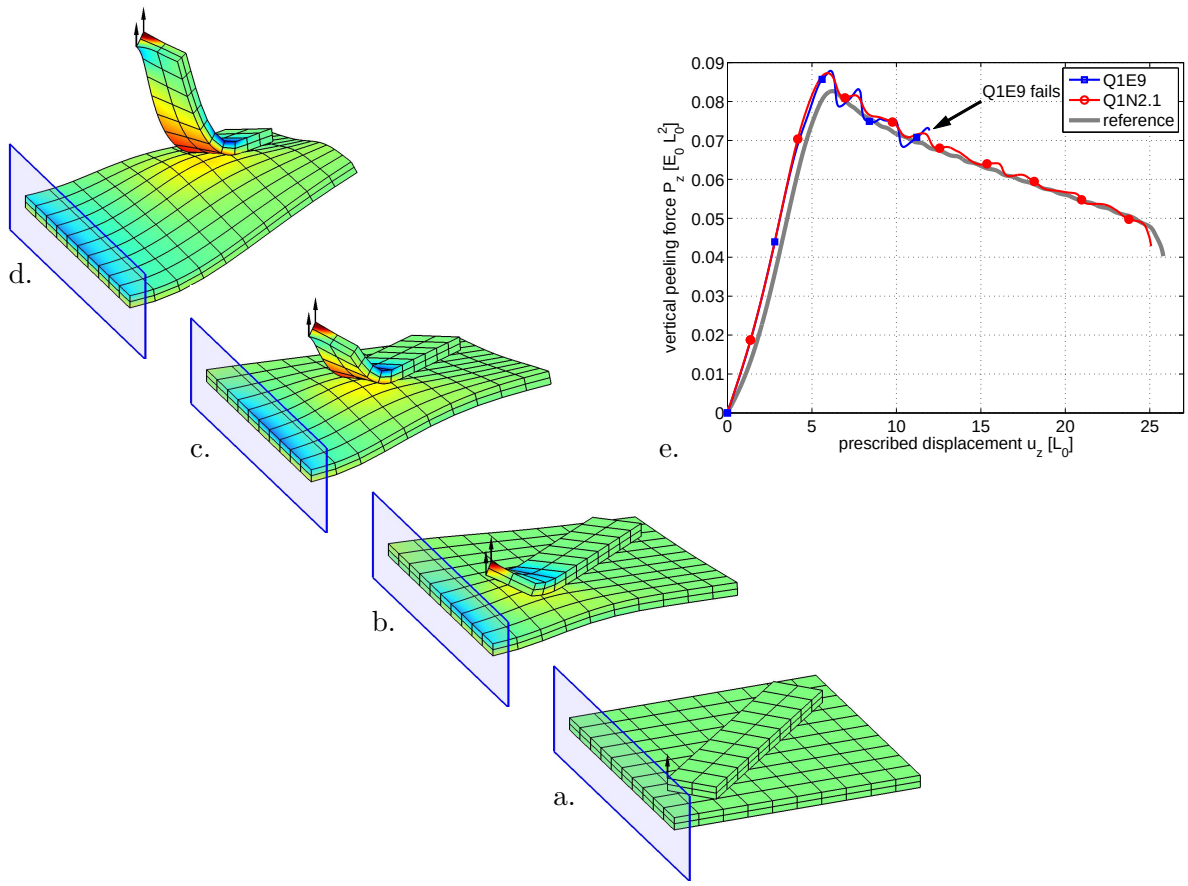

Figure 8: Finite element computation of the debonding between a flexible strip and plate (Corbett and Sauer, 2015): (a-d) deformation at displacement $u_z = 0, 3.2, 7.75, 15.5\, L_0$; (e) load-displacement curve for various FE discretizations.

2001) – and numerically – for arbitrary objects considering small deformations (Argento et al., 1997) or arbitrarily large deformations (Sauer and Li, 2007b). In principle, also other potentials can be integrated (Li et al., 2011a). The general framework involves the numerical integration over both bodies, which makes such a formulation very expensive. Therefore approximate methods are interesting that bring down the computational cost while maintaining the accuracy of the formulation. For certain deformations it is for example possible to transform the volume integrals of (41) into surface integrals (Sauer and Wriggers, 2009).

In the case of the Lennard Jones potential (40), the gradient of Π yields the traction-separation law given in (39). Such adhesion models have been essentially used in the numerical studies by Tworzydlo et al. (1998); Suh et al. (2004); Liu et al. (2006); Du et al. (2007); Sauer and Li (2007a); Kadin et al. (2008); Radhakrishnan and Mesarovic (2009); Sauer (2009b); Ardito et al. (2010); Eid et al. (2011b); Zhang et al. (2011); Jin et al. (2011); Ono (2012). Those computations often exploit approximations for the deformation or surface distance g_{n}. The surface distance can for example be approximated by taking it to be normal to the original tangent plane between the neighboring bodies, instead of taking the actual normal projection $\boldsymbol{n}_{\mathrm{p}}$ according to Fig. 5. This has been considered by Tworzydlo et al. (1998); Liu et al. (2006); Du et al. (2007); Kadin et al. (2008); Eid et al. (2011b); Zhang et al. (2011); Jin et al. (2011); Ono (2012). The approach is analogous to Derjaguin's approximation (Derjaguin, 1934; Israelachvili, 1991), which restricts the formulation to objects with curvature radii that are much larger than the range of interactions. Another simplification, sometimes considered in computations, is to approximately collocate the interaction to the FE nodes (Kadin et al., 2008; Ardito et al., 2010), thus skipping

the surface integration inherent to FE. Instead of the surface-based traction-separation law (39), the Lennard-Jones potential can also be used within a body force-based separation law. Examples are given in Cho and Park (2005), Sauer and Wriggers (2009), Bobji et al. (2010) and Jayadeep et al. (2014a,b). The last two references apply the formulation to study the adhesive impact of elastic rods and spheres, examining the apparent energy loss during impact.
The currently most general computational continuum formulation for van der Waals adhesion accounting for the actual surface distance and general, arbitrary deformations is the finite element formulation of Sauer and Li (2007b) and Sauer and Wriggers (2009). This formulation can also be used in conjuction with other potentials, like the Morse potential (Zeng and Li, 2011). It is also possible to unify the formulation for van der Waals adhesion and phenomenological traction laws with classical computational contact formulations (Sauer and De Lorenzis, 2013). Thus, the formulation can for example be used to study the normal and tangential debonding behavior of gecko spatulae, as is shown in Fig. 9. The example illustrates that structural effects

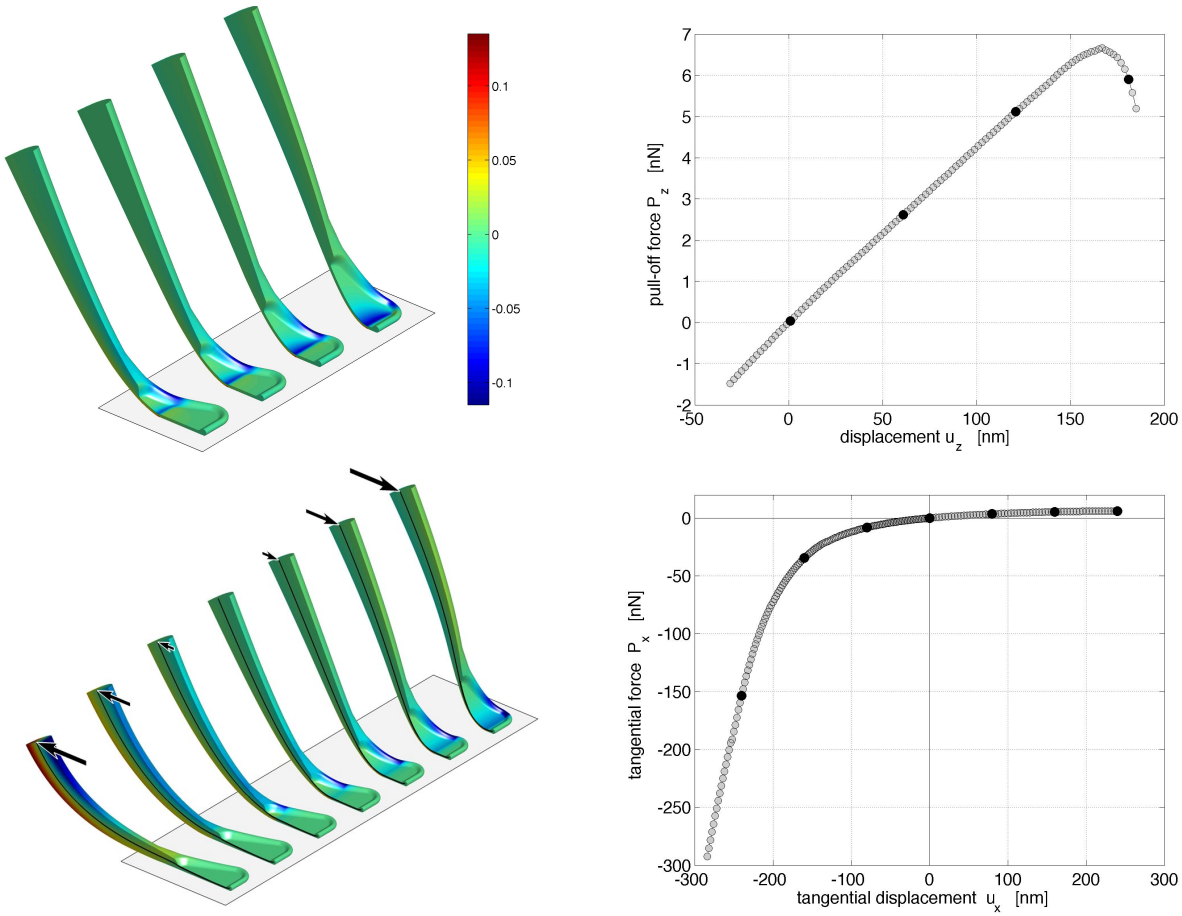

Figure 9: Finite element computation of the debonding of a gecko spatula: top: normal peeling (Sauer and Holl, 2013); bottom: tangential peeling (Sauer and Mergel, 2014). The black dots in the load displacement curves on the right hand side mark the spatula configurations shown on the left hand side. Due to symmetry, only half of the spatula is plotted. The color scale shows the stress $I_1 = \mathrm{tr}\,\boldsymbol{\sigma}$ in multiples of $E = 2\mathrm{GPa}$.

lead to strong anisotropy in the maximum peeling forces – about 6.6 nN for normal peeling, 6.1 nN for tangential peeling to the right and 295 nN for tangential peeling to the left – even though the molecular debonding model is fully isotropic.
Molecular potentials, like the Lennard-Jones potential, can also be used in molecular dynamics

(MD) simulations of adhesion, see for example Yongsheng et al. (1999); Gilabert et al. (2007); Peri and Cetinkaya (2009); Schmidt et al. (2014). Another possibility is to use detailed MD models in order to identify effective cohesive zone parameters for macro-scale applications. Examples can be found in Namilae and Chandra (2005); Yamakov et al. (2006); Zhou et al. (2009); Dandekar and Shin (2011); Krull and Yuan (2011); Paggi and Wriggers (2011); He and Li (2012); Paliwal and Cherkaoui (2013).

3.5.3 Electro-static interactions

The formulation of Eq. (41) can also by applied to other kinds of interactions, like for example electro-static interactions described by Coulomb's potential

$$\phi = c\,\frac{q_1\,q_2}{g}\ , \tag{42}$$

where c is Coulomb's constant, and where q_k is the electrical charge of volume element $\mathrm{d}v_k$. Those interactions can be quite long-ranging compared to the dimensions of the interacting bodies. Due to this, the full numerical integration of (41) must generally be considered. Corresponding finite element implementations are described in Sauer and Li (2007b) and Sauer and De Lorenzis (2013). Numerical examples for electro-static interactions are given in Shavezipur et al. (2011) and Sauer and De Lorenzis (2013).

3.5.4 Projection of material models onto the interface

Another possibility to construct traction-separation laws is to take the material models outlined in Sec. 2 and project them onto the interface. The 3D adhesive (with its 3D material law) is thus transformed into a 2D surface interaction model. Generally, this transformation will lead to a loss of some of the details of the original 3D model. The transformation is particularly useful for thin adhesive layers where the full 3D deformation state is not of interest. The approach has been considered in the work of Edlund and colleagues outlined in Sec. 2.3. It has also been considered recently in the context of soil friction by Weissenfels (2013). In general one has to integrate constitutive model $\boldsymbol{\sigma} = \boldsymbol{\sigma}(\boldsymbol{\varepsilon})$ over the adhesive layer $\mathcal{B}_\mathrm{i}$ to generate an effective traction-separation law of the form $\boldsymbol{t} = \boldsymbol{t}(\boldsymbol{g})$ (see Fig. 1). In the case of van der Waals adhesion a corresponding approach is given by the surface formulation presented in Sauer and Wriggers (2009).

3.5.5 Adhesive ligand-receptor binding of cells

Biological cell membranes contain proteins on the surface that can bond together. The interactions of these ligand and receptor proteins are governed by a kinetic reaction equation that models the formation and breaking of bonds. The interaction themselves are typical modeled by a simple linear spring (Bell, 1978; Bell et al., 1984). Denoting the interaction potential by ϕ, the total interaction energy of cell adhesion can be written as

$$\Pi = \int_{\Gamma_\mathrm{i}} \rho\,\phi\,\mathrm{d}a\ , \tag{43}$$

where ρ denotes the surface density of interactions on interface Γ_i. ρ is governed by a kinetic reaction equation – an ordinary differential equation of the form

$$\frac{\mathrm{d}\rho}{\mathrm{d}t} = f(\rho)\ . \tag{44}$$

Models for cell adhesion have for example been considered by Tozeren et al. (1989); Agresar (1996); N'Dri et al. (2003); Lin and Freund (2007); Liu et al. (2007); Pathak et al. (2008); Zhang and Zhang (2008); Li et al. (2011b); Wong and Tang (2011); Farsad and Vernerey (2012); Wei (2014). Further works can be found in the reference therein and in the review articles of Zhu (2000) and Sanz-Herrera and Reina-Romo (2011).

4 Effective models based on homogenization

The local, i.e. pointwise, adherent and adhesive models discussed so far can be homogenized into effective models describing the overall adhesion behavior of the entire system under investigation. The detailed interface and bulk relations $\boldsymbol{t} = \boldsymbol{t}(\boldsymbol{g})$ and $\boldsymbol{\sigma} = \boldsymbol{\sigma}(\boldsymbol{\varepsilon})$ are thus homogenized into an effective debonding relation governing the debonding forces and displacements between the adherents according to Fig. 1c. The procedure is essentially based on the integration (i.e. averaging) of the local material and interface models over their domains of interaction. In many cases – considering suitable approximations – this step can be evaluated analytically. Effective adhesion models can for example be used to construct hierarchical multiscale models for adhesion (Sauer, 2009b; Eid et al., 2011a). The following four cases are considered:

4.1 Adhesive contact of deformable spheres

The classical example of effective models are the adhesion models for elastic spheres of Johnson et al. (1971) and Derjaguin et al. (1975) – known as the JKR and DMT theories – that were later combined by Maugis (1992). The models are based on Hertzian contact, which in turn is based on the point load solution of half-space theory (Johnson, 1985), and on the concept of the work of adhesion (see Sec. 3.1). They are thus theoretically restricted to small deformations and small contact areas. But they can still come remarkably close to the full numerical solution of the unapproximated theory as is shown in Fig. 10. Those calculations are based on a finite element discretization of the general continuum problem considering Lennard-Jones interactions (Sauer and Li, 2007b). There are also other numerical formulations that are still based on half-space theory, e.g. see Muller et al. (1980); Attard and Parker (1992); Greenwood (1997); Feng (2000); Wu (2006, 2008). Computational approaches have also been used to investigate the scaling laws for sphere adhesion (Sauer and Li, 2008; Radhakrishnan and Mesarovic, 2009). The half-space adhesion theory has also been extended to elasto-plastic spheres (Mesarovic and Johnson, 2000) and flat punches (Ma et al., 2007). Effective adhesion models are often used to account for adhesion in granular interaction and flow (Liu et al., 2010; Li et al., 2011b; Nguyen et al., 2014).
Effective adhesion models have also been formulated for capillary adhesion, accounting for the global effect of liquid bridges, e.g. see Orr et al. (1975); Maugis (1987); Cai and Bhushan (2008). Due to the mathematical complexity of the Young-Laplace equation (33), these models are based on simplifications, like considering liquid bridges between rigid spheres, and assuming toroidal menisci.

4.2 Rough surface adhesion

Effective models have also been developed for rough surface contact and adhesion. Those go back to the classical multiasperity contact approach of Greenwood and Williamson (1966) – later extended by Bush et al. (1975) and Ciavarella et al. (2006) – that is based on local Hertzian contact together with a given, e.g. Gaussian, height distribution of the asperities. The

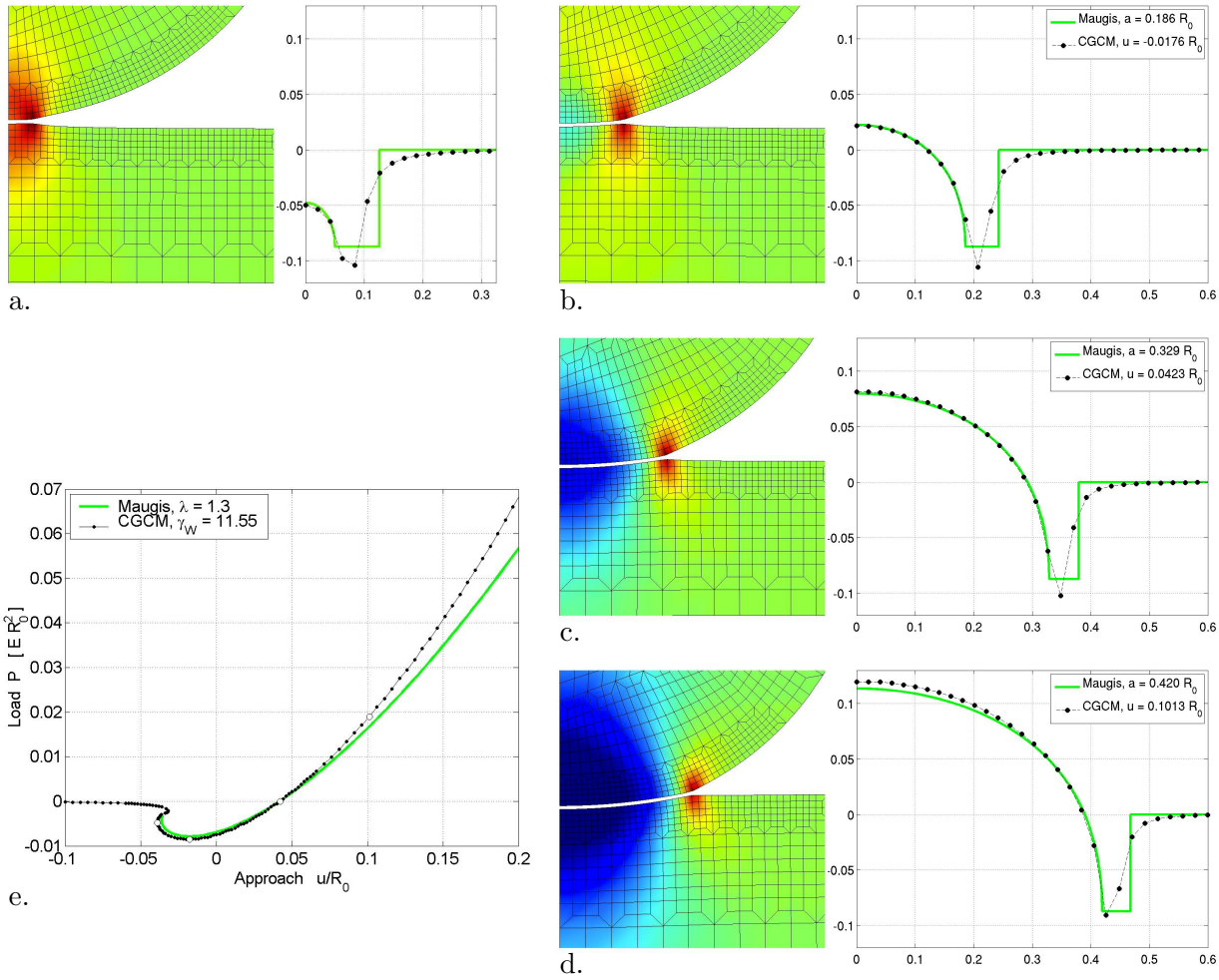

Figure 10: Adhesion of soft spheres (Sauer and Li, 2007a; Sauer, 2009a): (a-d) Deformation and stress field (left) and contact pressure (normalized by Young's modulus E) vs. radius (right) between a half-space and sphere with radius R_0; (e) load displacement curve, marking the four states shown in a.-d. by '$\circ$'. For small displacements, the theory of Maugis (1992) comes very close to the more general computational results.

formulation has been extended to adhesive, JKR-like contact by Fuller and Tabor (1975) and Johnson (1975), and DMT-like contact by Chang et al. (1988) and Maugis (1996). A drawback of the formulation is that it only accounts for roughness on one length scale. A further drawback of the underlying Hertzian and JKR-based contact models is that they are not applicable for full surface contact but only for locally small contact spots.

Full contact with a single-scale, periodic, wavy surface has been studied by Johnson (1995) – for the case of slight roughness – and by Zilberman and Persson (2002) – for the case of large roughness. The two cases were later combined by Sriwijaya et al. (2007).

A different approach, that accounts for roughness on several length scales and is also valid for full contact, is the rough surface contact theory of Persson (2001). The work has been extended to adhesive contact by Persson and Tosatti (2001) and Persson (2002).

In recent years the theories have been compared to numerical approaches based on finite element analysis (Hyun et al., 2004), Green's function and molecular dynamics (Campañá and Müser, 2007; Dapp et al., 2014), 2D boundary element methods (Carbone et al., 2009), non-linear elastic foundation theory (Galanov, 2011), and 3D surface integration (Medina and Dini, 2014).

Further theoretical and numerical studies of rough surface adhesion can be found in Hui et al. (2001); Carbone and Mangialardi (2004); Ali and Sahoo (2006); Sahoo (2006); Benz et al. (2006); Guduru (2007); Li and Kim (2009); Eid et al. (2011a) and Kesari and Lew (2011).
Effective models can also be formulated for capillary adhesion between rough surfaces. Streator and Jackson (2009) present a numerical model for capillary adhesion between deformable 2D rough surfaces, based on the analytical half-space model of Zheng and Streator (2004).

4.3 Computational peeling models for thin elastic films

Another popular field where effective adhesion models have been developed is thin film peeling. Effective peeling models provide a relation for the maximum peeling force based on the model parameters like the peeling angle, film stiffness, and work of adhesion. The initial model of this kind was derived by Kendall (1975). Since then, the formulation has been extended to account for root rotation and plasticity (Williams, 1993), shear and bending stiffness (Li et al., 2004; Thouless and Yang, 2008), Lennard-Jones based adhesion (Oyharcabal and Frisch, 2005), nonlinear material behavior (Williams and Kauzlarich, 2005; Molinari and Ravichandran, 2008), interfacial slippage (Lu et al., 2007), the deformation in the peeling zone (Pesika et al., 2007), pre-straining and pre-tensioning (Molinari and Ravichandran, 2008; Chen et al., 2009), and interface sliding (Collino et al., 2014). Recently, a geometrically exact beam formulation has been developed for peeling that accounts for varying film thickness and captures the bending and shear deformation due to adhesion (Sauer, 2011c; Sauer and Mergel, 2014). The formulation can be evaluated very efficienctly with finite beam elements (Sauer and Mergel, 2014). Such a formulation is ideal to study shape optimization of peeling strips (Mergel et al., 2014; Mergel and Sauer, 2014). Of course, peeling can also be analyzed with a standard finite element approach based on continuum theory, e.g. see Crocombe and Adams (1981); Wei (2004) or Thouless and Yang (2008). However, in the case of peeling, such model can be much less efficient while not being more accurate.

4.4 Computational models for fibrillar adhesives

The natural adhesion mechanism of many insects and lizards often has a hierarchical and fibrillar microstructure: slender fibers that branch into finer fibers that are capable to adhere to rough surfaces. A system that has received particular attention is the adhesion mechanism of the gecko. Gecko feet are covered with hundreds of thousand micrometer fine hair known as setae, which branch into even finer hair terminating into nanometer-scale tips known as spatulae. These spatulae can adhere to neighboring surfaces due to van der Waals and capillary interactions (Autumn et al., 2002; Huber et al., 2005). From animal scale to molecular scale, the mechanism spans nine orders of magnitude. The theoretical and numerical analysis of fibrillar gecko adhesion mechanisms goes back to the works of Persson (2003) and Gao et al. (2005). Simple fractal models for the hierarchical adhesive microstructures have been studied by Tang et al. (2005); Bhushan et al. (2006); Yao and Gao (2006, 2007); Kim and Bhushan (2007a,b) and extended to account for capillary adhesion (Kim and Bhushan, 2008), tilting of the fibrils (Schargott, 2009), and multiscale modeling for static (Sauer, 2009b) and dynamic (Sauer, 2010) seta detachment. A recent review of gecko adhesion has been provided by Kwaki and Kim (2010). Sometimes, the JKR and Kendall models are considered to study gecko adhesion, although these models are not suitable for many fibrillar microstructures, simply because the fibers often don't observe the assumptions inherent to those models (Sauer, 2011c). In order to model the adhesive tips of fibrillar microstructures therefore often detailed, 3D models are used (Dai and Gorb, 2009; Pantano et al., 2011; Sauer and Holl, 2013). Due to the involvement

of many length scales, different models at different length scales are typically needed to study fibrillar adhesives (Sauer, 2014a). The slender fibrils can for example be modeled efficiently by beam theory (Sauer and Mergel, 2014), which is used in the computations shown in Fig. 9. Recently the modeling of entire fiber arrays has also been considered (Gillies and Fearing, 2014).

5 Conclusion

This paper provides a survey of computational methods for adhesive contact focusing on general continuum mechanical models for the attractive adhesion of solids. The aim is to provide a complete overview of the formulations and methods suitable for computational modeling. The survey distinguishes between local material models (Sec. 2), local interface models (Sec. 3) and effective models (Sec. 4) for adhesion. Local material models describe the local stress-strain behavior within the adhesive due to local elasticity, viscosity, plasticity, fracturing, damage and thermal, curing and ageing effects. For liquid adhesives also capillary forces due to surface tension can play an important role. Local interface models describe the local traction-separation behavior at the material interface. This behavior can be related to strong or weak molecular bonds, electrostatic interactions, or phenomenological fracture and debonding models. This framework can therefore account for all adhesion mechanisms. Effective adhesion models describe the effective debonding and bonding at the global level, for example in the form of global load-displacement curves. Examples are adhesion models for spheres, rough surfaces, thin films and fibrillar microstructures.

While there is a lot a work to be found on the modeling and computation of adhesive contact, there are still several important aspects that would greatly benefit from further research. One such aspect is the coupling of different models, for example to describe the durability of adhesive joints under nonlinear mechanical, thermal and corrosive influences. For this, experimental investigations are called for that go well beyond standard test cases. Such experiments then serve as important benchmark case to determine, calibrate and validate suitable analytical and computational models.

Acknowledgements

The author is grateful to the German Research Foundation (DFG) for supporting this research under projects SA1822/5-1 and GSC 111. The author also wishes to thank the graduate students Thang X. Duong and Ajay Rangarajan for their help in tracking down the literature.

References

Adams, R. D. and Peppiatt, N. A. (1974). Stress analysis of adhesive-bonded lap joints. *J. Strain Anal.*, **9**(3):185–196.

Adolf, D. and Martin, J. E. (1996). Calculation of stresses in crosslinked polymers. *J. Compos. Mater.*, **30**:13–34.

Agrawal, A. (2011). Mechanics of membrane-membrane adhesion. *Math, Mech. Solids*, **16**(8):872–886.

Agresar, G. (1996). *A computational environment for the study of circulating cell mechanics and adhesion*. PhD thesis, University of Michigan, Ann Arbor, USA.

Ahn, J. (2008). Thick obstacle problems with dynamic adhesive contact. *ESAIM, Math. Model. Numer. Anal.*, **42**(6):1021–1045.

Aksak, B., Murphy, M. P., and Sitti, M. (2007). Adhesion of biologically inspired vertical and angled polymer microfiber arrays. *Langmuir*, **23**:3322–3332.

Ali, S. M. and Sahoo, P. (2006). Adhesive friction for elastic-plastic contacting rough surfaces using a scale-dependent model. *J. Phys. D: Appl. Phys.*, **39**(4):721–729.

Allix, O. and Ladevèze, P. (1992). Interlaminar interface modelling for the prediction of delamination. *Composite Struct.*, **22**:235–242.

Anderson, G. P., DeVries, K. L., and Williams, M. L. (1973). Finite element in adhesion analyses. *Int. J. Fract.*, **9**(4):421–436.

Andersson, T. and Biel, A. (2006). On the effective constitutive properties of a thin adhesive layer loaded in peel. *Int. J. Frac.*, **141**:227–246.

Andersson, T. and Stigh, U. (2004). The stresselongation relation for an adhesive layer loaded in peel using equilibrium of energetic forces. *Int. J. Solids Struct.*, **41**:413–434.

André, M. and Wriggers, P. (2005). Thermo-mechanical behavior of rubber materials during vulcanization. *Int. J. Solids Struct.*, **42**:4758–4778.

Andrews, K. T., Chapman, L., Fernández, J. R., Fisackerly, M., Shillor, M., Vanerian, L., and VanHouten, T. (2003). A membrane in adhesive contact. *SIAM J. Appl. Math.*, **64**(1):152–169.

Andruet, R. H., Dillard, D. A., and Holzer, S. M. (2001). Two- and three-dimensional geometrical nonlinear finite elements for analysis of adhesive joints. *Int. J. Adhesion Adhesives*, **21**:17–34.

Apalak, M. K. and Engin, A. (1997). Geometrically non-linear analysis of adhesively bonded double containment cantilever joints. *J. Adhesion Sci. Technol.*, **11**(9):1153–1195.

Ardito, R., Corigliano, A., and Frangi, A. (2010). Multiscale finite-element models for predicting spontaneous adhesion in MEMS. *Mécanique & Industries*, **11**(3-4):177–182.

Argento, C., Jagota, A., and Carter, W. C. (1997). Surface formulation for molecular interactions of macroscopic bodies. *J. Mech. Phys. Solids*, **45**(7):1161–1183.

Armstrong, N. J., Painter, K. J., and Sherratt, J. A. (2006). A continuum approach to modelling cell-cell adhesion. *J. Theor. Biol.*, **243**:98–113.

Arzt, E., Gorb, S., and Spolenak, R. (2003). From micro to nano contacts in biological attachment devices. *Proc. Natl. Acad. Sci. USA*, **100**(19):10603–10606.

Ashcroft, I. A. (2011). Fatigue load conditions. In da Silva, L. F. M., Öchsner, A., and Adams, R. D., editors, *Handbook of Adhesion Technology*, pages 845–874. Springer.

Ashcroft, I. A. and Comyn, J. (2011). Effect of water and mechanical stress on durability. In da Silva, L. F. M., Öchsner, A., and Adams, R. D., editors, *Handbook of Adhesion Technology*, pages 789–822. Springer.

Ashcroft, I. A. and Crocombe, A. D. (2013). Prediction of joint strength under humid conditions: Damage mechanics approach. In da Silva, L. F. M. and Sato, C., editors, *Design of Adhesive Joints Under Humid Conditions*, pages 123–146. Springer.

Attard, P. and Parker, J. L. (1992). Deformation and adhesion of elastic bodies in contact. *Phys. Rev. A*, **46**:7959–7971.

Autumn, K. and Peattie, A. M. (2002). Mechanisms of adhesion in geckos. *Integr. Comp. Biol.*, **42**:1081–1090.

Autumn, K., Sitti, M., Liang, Y. A., Peattie, A. M., Hansen, W. R., Sponberg, S., Kenny, T. W., Fearing, R., Israelachvili, J., and Full, R. J. (2002). Evidence for van der Waals adhesion in gecko seta. *Proc. Natl. Acad. Sci. USA.*, **99**(19):12252–12256.

Bambach, M., Pietryga, M., Mikloweit, A., and Hirt, G. (2014). A finite element framework for the evolution of bond strength in joining-by-forming processes. *J. Mater. Proces. Technol.*, **214**:2156–2168.

Banea, M. D. and da Silva, L. F. M. (2009). Adhesively bonded joints in composite materials: an overview. *P. I. Mech. Eng. L – J. Mat.*, **223**(L1):1–18.

Bell, G. I. (1978). Models for the specific adhesion of cells to cells. *Science*, **200**:618–627.

Bell, G. I., Dembo, M., and Bongrand, P. (1984). Cell adhesion – Competition between non-specific repulsion and specific bonding. *Biophys. J.*, **45**:1051–1064.

Belytschko, T., Gracie, R., and Ventura, G. (2009). A review of extended/generalized finite elementcmethods for material modeling. *Model. Simul. Mater. Sci. Eng.*, **17**:043001.

Belytschko, T., Liu, W. K., and Moran, B. (2000). *Nonlinear Finite Elements for Continua and Structures*. Wiley.

Benz, M., Rosenberg, K. J., Kramer, E. J., and Israelachvili, J. N. (2006). The deformation and adhesion of randomly rough and patterned surfaces. *J. Phys. Chem. B*, **110**(24):11884–11893.

Bhushan, B., Peressadko, A. G., and Kim, T.-W. (2006). Adhesion analysis of two-level hierarchical morphology in natural attachment systems for 'smart adhesion'. *J. Adhesion Sci. Technol.*, **20**(13):1475–1491.

Blossey, R. (2003). Self-cleaning surfaces - virtual realities. *Nat. Mater.*, **2**:301–306.

Bobji, M. S., Xavier, S., Jayadeep, U. B., and Jog, C. S. (2010). Adhesion-induced instability in asperities. *Tribol. Lett.*, **39**:201–209.

Bonetti, E., Bonfanti, G., and Rossi, R. (2008). Global existence for a contact problem with adhesion. *Math. Meth. Appl. Sci.*, **31**:1029–1064.

Bonetti, E., Bonfanti, G., and Rossi, R. (2009). Thermal effects in adhesive contact: modelling and analysis. *Nonlinearity*, **22**:2697–2731.

Bonetti, E., Bonfanti, G., and Rossi, R. (2012). Analysis of a unilateral contact problem taking into account adhesion and friction. *J. Differential Equations*, **253**:438–462.

Borden, M. J., Scott, M. A., Evans, J. A., and Hughes, T. J. R. (2011). Isogeometric finite element data structures based on Bezier extraction of NURBS. *Int. J. Numer. Meth. Engng.*, **87**:15–47.

Borg, R., Nilsson, L., and Simonsson, K. (2002). Modeling of delamination using a discretized cohesive zone and damage formulation. *Compos. Sci. Technol.*, **62**(10-11):1299–1314.

Bradley, R. S. (1932). The cohesive force between solid surfaces and the surface energy of solids. *Phil. Mag.*, **13**:853–862.

Brakke, K. A. (1992). The surface evolver. *Experimental Mathematics*, **1**(2):141–165.

Brown, R. A., Orr, F. M., and Scriven, L. E. (1980). Static drop on an inclined plate: Analysis by the finite element method. *J. Colloid Interface Sci.*, **73**(1):76–87.

Bush, A. W., Gibson, R. D., and Thomas, T. R. (1975). The elastic contact of a rough surface. *Wear*, **35**:87–111.

Cai, S. and Bhushan, B. (2008). Meniscus and viscous forces during separation of hydrophilic and hydrophobic surfaces with liquid-mediated contacts. *Mat. Sci. Eng. R*, **61**(1-6):78–106.

Camacho, G. T. and Ortiz, M. (1996). Computational modelling of impact damage in brittle materials. *Int. J. Solids Struct.*, **33**:2899–2938.

Campañá, C. and Müser, M. H. (2007). Contact mechanics of real vs. randomly rough surfaces: A Green's function molecular dynamics study. *EPL*, **77**:38005.

Campilho, R. D. S. G., Banea, M. D., Pinto, A. M. G., da Silva, L. F. M., and de Jesus, A. M. P. (2011). Strength prediction of single- and double-lap joints by standard and extended finite element modelling. *Int. J. Adhesion Adhesives*, **31**(5):363–372.

Carbone, G. and Mangialardi, L. (2004). Adhesion and friction of an elastic half-space in contact with a slightly wavy rigid surface. *J. Mech. Phys. Solids*, **52**(6):1267–1287.

Carbone, G., Scaraggi, M., and Tartaglino, U. (2009). Adhesive contact of rough surfaces: Comparison between numerical calculations and analytical theories. *Eur. Phys. J. E*, **30**(1):65–74.

Carpenter, W. C. (1990). Viscoelastic analysis of bonded connections. *Comput. Struc.*, **36**(6):1141–1152.

Carpinteri, A., Paggi, M., and Zavarise, G. (2008). The effect of contact on the decohesion of laminated beams with multiple microcracks. *Int. J. Solids Struc.*, **45**:129–143.

Chang, W. R., Etsion, L., and Bogy, D. B. (1988). Adhesion model for metallic rough surfaces. *J. Trib.*, **110**:50–56.

Chau, O., Fernández, J. R., Shillor, M., and Sofonea, M. (2003). Variational and numerical analysis of a quasistatic viscoelastic contact problem with adhesion. *J. Comput. Appl. Math.*, **159**:431–465.

Chen, B., Wu, P., and Gao, H. (2009). Pre-tension generates strongly reversible adhesion of a spatula pad on substrate. *J. R. Soc. Interface*, **6**(2065):529–537.

Cho, S.-S. and Park, S. (2005). Finite element modeling of adhesive contact using molecular potential. *Tribol. Int.*, **37**:763–769.

Ciavarella, M., Delfine, V., and Demelio, G. (2006). A re-vitalized Greenwood and Williamson model of elastic contact between fractal surfaces. *J. Mech. Phys. Solids*, **54**:2569–2591.

Cocou, M. and Rocca, R. (2000). Existence results for unilateral quasistatic contact problems with friction and adhesion. *Math. Model. Numer. Anal.*, **34**(5):981–1001.

Cocou, M., Schryve, M., and Raous, M. (2010). A dynamic unilateral contact problem with adhesion and friction in viscoelasticity. *Z. Angew. Math. Phys.*, **61**:721–743.

Collino, R. R., Philips, N. R., Rossol, M. N., McMeeking, R. M., and Begley, M. R. (2014). Detachment of compliant films adhered to stiff substrates via van der Waals interactions: role of frictional sliding during peeling. *J. R. Soc. Interface*, **11**:20140453.

Comyn, J. (1997). *Adhesion Science*. Royal Society of Chemistry Paperbacks.

Comyn, J. (2011). Thermal properties of adhesives. In da Silva, L. F. M., Öchsner, A., and Adams, R. D., editors, *Handbook of Adhesion Technology*, pages 415–442. Springer.

Comyn, J. (2013). Diffusion of water in adhesives. In da Silva, L. F. M. and Sato, C., editors, *Design of Adhesive Joints Under Humid Conditions*, pages 1–19. Springer.

Corbett, C. J. and Sauer, R. A. (2014). NURBS-enriched contact finite elements. *Comput. Methods Appl. Mech. Engrg.*, **275**:55–75.

Corbett, C. J. and Sauer, R. A. (2015). Three-dimensional isogeometrically enriched finite elements for mixed-mode contact and debonding. *Comput. Methods Appl. Mech. Engrg.*, **284**:781–806.

Cottrell, J. A., Hughes, T. J. R., and Bazilevs, Y. (2009). *Isogeometric Analysis*. Wiley.

Créac'hcadec, R. and Cognard, J. Y. (2009). 2-D modeling of the behavior of an adhesive in an assembly using a non-associated elasto-visco-plastic model. *J. Adhes.*, **85**(4-5):239–260.

Créac'hcadec, R., Cognard, J. Y., and Heuzé, T. (2008). On modelling the non-linear behaviour of thin adhesive films in bonded assemblies with interface elements. *J. Adhes. Sci. Tech.*, **22**:1541–1563.

Crisfield, M. A. and Alfano, G. (2002). Adaptive hierarchical enrichment for delamination fracture using a decohesive zone model. *Int. J. Numer. Meth. Engrg.*, **54**(9):1369–1390.

Crocombe, A. D. and Adams, R. D. (1981). Peel analysis using the finite element method. *J. Adhesion*, **12**:127–139.

Crocombe, A. D. and Ashcroft, I. A. (2013). Prediction of joint strength under humid conditions with cyclic loading. In da Silva, L. F. M. and Sato, C., editors, *Design of Adhesive Joints Under Humid Conditions*, pages 147–182. Springer.

Cui, J., Wang, R., Sinclair, A. N., and Spelt, J. K. (2003). A calibrated finite element model of adhesive peeing. *Int. J. Adhesion Adhesives*, **23**:199–206.

Dai, Z. and Gorb, S. (2009). Contact mechanics of pad of grasshopper (Insecta: Orthoptera) by finite element methods. *Chinese Sci. Bulletin*, **54**(4):549–555.

Dandekar, C. R. and Shin, Y. C. (2011). Molecular dynamics based cohesive zone law for describing Al-SiC interface mechanics. *Composites A*, **42**:355–363.

Dapp, W. B., Prodanov, N., and Müser, H. (2014). Systematic analysis of Perssons contact mechanics theory of randomly rough elastic surfaces. *J. Phys.: Condens. Matter*, **26**:355002.

De Lorenzis, L. and Zavarise, G. (2008). Modeling of mixed mode debonding in the peel test applied to superficial reinforcements. *Int. J. Solids Struc.*, **45**:5419–5436.

de Moura, M. F. S. F., Gonçalves, J. P. M., and Magalhães, A. G. (2012). A straightforward method to obtain the cohesive laws of bonded joints under mode I loading. *Int. J. Adhesion Adhesives*, **39**:54–59.

Del Piero, G. and Raous, M. (2010). A unified model for adhesive interfaces with damage, viscosity, and friction. *Eur. J. Mech. A-Solid*, **29**:496–507.

Derjaguin, B. V. (1934). Untersuchungen über die Reibung und Adhäsion: IV. Theorie des Anhaftens kleiner Teilchen. *Kolloid Z.*, **69**:155–164.

Derjaguin, B. V., Muller, V. M., and Toporov, Y. P. (1975). Effect of contact deformation on the adhesion of particles. *J. Colloid Interface Sci.*, **53**(2):314–326.

Destuynder, P., Michavila, F., Santos, A., and Ousset, Y. (1992). Some theoretical aspects in computational analysis of adhesive lap joints. *Int. J. Numer. Meth. Engng.*, **35**:1237–1262.

Diehl, T. (2008). On using a penalty-based cohesive-zone finite element approach, Part I: Elastic solution benchmarks. *Int. J. Adhesion Adhesives*, **28**:237–255.

Dillard, D. A. (2011). Physical properties of adhesives. In da Silva, L. F. M., Öchsner, A., and Adams, R. D., editors, *Handbook of Adhesion Technology*, pages 393–414. Springer.

Dimitri, R., Lorenzis, L. D., Wriggers, P., and Zavarise, G. (2014). NURBS- and T-spline-based isogeometric cohesive zone modeling of interface debonding. *Comput. Mech.*, **54**(2):369–388.

Du, Y., Chen, L., McGruer, N. E., Adams, G. G., and Etsion, I. (2007). A finite element model of loading and unloading of an asperity contact with adhesion and plasticity. *J. Colloid Interf. Sci.*, **312**(2):522–528.

Edlund, U. (1994). Surface adhesive joint description with coupled elastic-plastic damage behaviour and numerical applications. *Comput. Meth. Appl. Mech. Engrg.*, **115**:253–276.

Edlund, U. and Klarbring, A. (1990). Analysis of elastic and elastic-plastic adhesive joints using a mathematical programming approach. *Comput. Meth. Appl. Mech. Engrg.*, **78**:19–47.

Edlund, U. and Klarbring, A. (1992). A geometrically nonlinear model of the adhesive joint problem and its numerical treatment. *Comput. Meth. Appl. Mech. Engrg.*, **96**:329–350.

Edlund, U. and Klarbring, A. (1993). A coupled elasto-plastic damage model for rubber-modified epoxy adhesives. *Int. J. Solids Struct.*, **30**(19):2693–2708.

Eid, H., Adams, G. G., McGruer, N. E., Fortini, A., Buldyrev, S., and Srolovitz, D. (2011a). A combined molecular dynamics and finite element analysis of contact and adhesion of a rough sphere and a flat surface. *Tribol. Trans.*, **54**:920–928.

Eid, H., Joshi, N., McGruer, N. E., and Adams, G. G. (2011b). A model of contact with adhesion of a layered elastic-plastic microsphere with a rigid flat surface. *J. Tribol.*, **133**:031406.

Eligehausen, R., Popov, E. P., and Bertéro, V. V. (1983). *Local bond stress-slip relationships of deformed bars under generalized excitations.* Report No. UCB/EERC-83/23, University of California, Berkeley.

Elmukashfi, E. and Kroon, M. (2014). Numerical analysis of dynamic crack propagation in biaxially strained rubber sheets. *Eng. Frac. Mech.*, **124-125**:1–17.

Farsad, M. and Vernerey, F. J. (2012). An XFEM-based numerical strategy to model mechanical interactions between biological cells and a deformable substrate. *Int. J. Numer. Meth. Engrg.*, **92**(3):238–267.

Feng, J. Q. (2000). Contact behavior of spherical elastic particles: a computational study of particle adhesion and deformation. *Colloid Surf. A*, **172**(1-2):175–198.

Feng, X.-Q., Li, H., Zhao, H.-P., and Yu, S.-W. (2009). Numerical simulations of the normal impact of adhesive microparticles with a rigid substrate. *Powder Tech.*, **189**(1):34–41.

Fernandes, R. M. R. P., Chousal, J. A. G., de Moura, M. F. S. F., and Xavier, J. (2013). Determination of cohesive laws of composite bonded joints under mode II loading. *Composites B*, **52**:269–274.

Fernández, J. R., Shillor, M., and Sofonea, M. (2003). Analysis and numerical simulations of a dynamic contact problem with adhesion. *Math. Comput. Model.*, **37**:1317–1333.

Fogelson, A. L. (1984). A mathematical model and numerical method for studying platelet adhesion and aggregation during blood clotting. *J. Comput. Phys.*, **56**:111–134.

Fremond, M. (1988). Contact with adhesion. In Moreau, J. J. and Panagiotopoulos, P. D., editors, *Nonsmooth Mechanics and Applications*, pages 177–221. Springer.

Fries, T.-P. and Belytschko, T. (2010). The extended/generalized finite element method: An overviewcof the method and its applications. *Int. J. Numer. Mech. Engng.*, **84**:253–304.

Fuller, K. N. G. and Tabor, D. (1975). The effect of surface roughness on the adhesion of elastic solids. *Proc. R. Soc. Lond. A*, **345**:327–342.

Galanov, B. A. (2011). Models of adhesive contact between rough elastic solids. *Int. J. Mech. Sci.*, **53**(11):968–977.

Gao, H., Wang, X., Yao, H., Gorb, S., and Arzt, E. (2005). Mechanics of hierarchical adhesion structures of geckos. *Mech. Mater.*, **37**:275–285.

Gautam, S. S. and Sauer, R. A. (2013). An energy-momentum-conserving temporal discretization scheme for adhesive contact problems. *Int. J. Numer. Meth. Engrg.*, **93**(10):1057–1081.

Gautam, S. S. and Sauer, R. A. (2014). A composite time integration scheme for dynamic adhesion and its application to gecko spatula peeling. *Int. J. Comput. Methods*, **11**(5):1350104.

Ge, L., Sethi, S., Ci, L., Ajayan, P. M., and Dhinojwala, A. (2007). Carbon nanotube-based synthetic gecko tapes. *Proc. Natl. Acad. Sci. USA*, **104**(26):10792–10795.

Gerberich, W. W. and Cordill, M. J. (2006). Physics of adhesion. *Rep. Prog. Phys.*, **69**:2157–2203.

Ghatak, A., Mahadevan, L., Chung, J. Y., Chaudhury, M. K., and Shenoy, V. (2004). Peeling from a biomimetically patterned thin elastic film. *Proc. R. Soc. Lond. A*, **460**:2725–2735.

Gilabert, F. A., Quintanilla, M. A. S., Castellanos, A., and Valverde, J. M. (2007). Adhesive elastic plastic contact: theory and numerical simulation. *Zeitschrift für Angewandte Mathematik und Mechanik*, **87**(2):128–138.

Gillies, A. G. and Fearing, R. S. (2014). Simulation of synthetic gecko arrays shearing on rough surfaces. *J. R. Soc. Interface*, **11**:20140021.

Gorb, S., Varenberg, M., Peressadko, A., and Tuma, J. (2007). Biomimetic mushroom-shaped fibrillar adhesive microstructure. *J. R. Soc. Interface*, **4**:271–275.

Greenwood, J. A. (1997). Adhesion of elastic spheres. *Proc. R. Soc. Lond. A*, **453**:1277–1297.

Greenwood, J. A. and Williamson, J. B. P. (1966). Contact of nominally flat surfaces. *Proc. Roy. Soc. A*, **295**(1442):300–319.

Gross, D. and Seelig, T. (2006). *Fracture Mechanics*. Springer.

Gruttmann, F. and Pham, V. D. (2008). A finite element model for the analysis of buckling driven delamination of thin films on rigid substrates. *Comp. Mech.*, **41**(3):361–370.

Gu, R., Wang, X., and Gunzburger, M. (2014). Simulating vesicle-substrate adhesion using two phase field functions. *J. Comp. Phys.*, **275**:626–641.

Guduru, P. R. (2007). Detachment of a rigid solid from an elastic wavy surface: Theory. *J. Mech. Phys. Solids*, **55**:445–472.

Guiamatsia, I., Ankersen, J. K., Davies, G. A. O., and Iannucci, L. (2009). Decohesion finite element with enriched basis functions for delamination. *Compos. Sci. Technol.*, **69**(15-16):2616–2624.

Hamaker, H. C. (1937). The London–van der Waals attraction between spherical particles. *Physica*, **4**(10):1058–1072.

Han, W., Kuttler, K. L., Shillor, M., and Sofonea, M. (2002). Elastic beam in adhesive contact. *Int. J. Solids Struc.*, **39**:1145–1164.

He, M. and Li, S. (2012). An embedded atom hyperelastic constitutive model and multiscale cohesive finite element method. *Comput. Mech.*, **49**:337–355.

He, X. (2011). A review of finite element analysis of adhesively bonded joints. *Int. J. Adhesion Adhesives*, **31**:248–264.

Hendrickx, J. M., Geubelle, P. H., and Sottos, N. R. (2005). A spectral scheme for the simulation of dynamic mode 3 delamination of thin films. *Eng. Frac. Mech.*, **72**(12):1866–1891.

Holzapfel, G. A. (2000). *Nonlinear Solid Mechanics: A Continuum Approach for Engineering*. Wiley.

Hossain, M., Possart, G., and Steinmann, P. (2009). Finite strain framework for the simulation of polymer curing. part I: Elasticity. *Comput. Mech.*, **44**(5):621–630.

Hossain, M., Possart, G., and Steinmann, P. (2010). Finite strain framework for the simulation of polymer curing. part II: Viscoelasticity and shrinkage. *Comput. Mech.*, **46**:363–375.

Huber, G., Mantz, H., Spolenak, R., Mecke, K., Jacobs, K., Gorb, S. N., and Arzt, E. (2005). Evidence for capillarity contributions to gecko adhesion from single spatula nanomechanical measurements. *Proc. Natl. Acad. Sci. USA*, **102**(45):16293–16296.

Hui, C. Y., Lin, Y. Y., Baney, J. M., and Kramer, E. J. (2001). The mechanics of contact and adhesion of periodically rough surfaces. *J. Polymer Sci. B: Polymer Phys.*, **39**:1195–1214.

Hunter, R., Ibacache, N., Möller, J., Betancourt, R., Mora, T., Diez, E., and Pavez, B. (2012). Influence of roughness on the mechanical adhesion of single lap joints. *J. Adhes.*, **88**(4-6):376–390.

Hyun, S., Pei, L., J.-F-Molinari, and Robbins, M. O. (2004). Finite-element analysis of contact between elastic self-affine surfaces. *Phys. Rev. E*, **70**(2):026117.

Iliev, S. D. (1995). Iterative method for shape of static drops. *Computer Methods in Applied Mechanics and Engineering*, **126**:251–265.

Israelachvili, J. N. (1991). *Intermolecular and Surface Forces*. Academic Press, 2nd edition.

Jayadeep, U. B., Bobji, M. S., and Jog, C. S. (2014a). Energy loss due to adhesion in longitudinal impact of elastic cylinders. *Eur. J. Mech. A/Solids*, **45**:20–31.

Jayadeep, U. B., Bobji, M. S., and Jog, C. S. (2014b). Energy loss in the impact of elastic spheres on a rigid half-space in presence of adhesion. *Tribol. Lett*, **53**:79–89.

Ji, G., Ouyang, Z., and Li, G. (2011). Effects of bondline thickness on mode-ii interfacial laws of bonded laminated composite plate. *Int J. Fract.*, **168**:197–207.

Jin, C., Jagota, A., and Hui, C.-Y. (2011). An easy-to-implement numerical simulation method for adhesive contact problems involving asymmetric adhesive contact. *J. Phys. D: Appl. Phys.*, **44**:405303.

Johnson, K. L. (1975). Non-Hertzian contact of elastic spheres. In De Pater, A. D. and Kalker, J. J., editors, *The Mechanics of the Contact Between Deformable Bodies*, pages 26–40. Delft University Press.

Johnson, K. L. (1985). *Contact Mechanics*. Cambridge University Press.

Johnson, K. L. (1995). The adhesion of two elastic bodies with slightly wavy surfaces. *Int. J. Solids Structures*, **32**(3/4):423–430.

Johnson, K. L., Kendall, K., and Roberts, A. D. (1971). Surface energy and the contact of elastic solids. *Proc. R. Soc. Lond. A*, **324**:301–313.

Kadin, Y., Kligerman, Y., and Etsion, I. (2008). Loading-unloading of an elasticplastic adhesive spherical microcontact. *J. Colloid Interface Sci.*, **321**:242–250.

Kaziolas, D. N., Kontoleon, M. J., Koltsakis, E. K., and Panagiotopoulos, P. D. (2000). Three-dimensional adhesive contact laws with debonding: a nonconvex energy bundle method. *Comput. Meth. Appl. Mech. Engrg.*, **186**(1):23–48.

Kendall, K. (1975). Thin-film peeling – the elastic term. *J. Phys. D: Appl. Phys.*, **8**:1449–1452.

Kendall, K., Amal, R., Jiang, X., and Yu, A. (2007). Effect of adhesion on aggregation in nanoparticle dispersions. *J. Adhes.*, **83**:573–585.

Kesari, H. and Lew, A. J. (2011). Effective macroscopic adhesive contact behavior induced by small surface roughness. *J. Mech. Phys. Solids*, **59**:2488–2510.

Kim, D. S., Lee, H. S., Lee, J., Kim, S., Lee, K.-H., Moon, W., and Kwon, T. H. (2007). Replication of high-aspect-ratio nanopillar array for biomimetic gecko foot-hair prototype by UV nano embossing with anodic aluminum oxide mold. *Microsyst. Technol*, **13**:601–606.

Kim, T. W. and Bhushan, B. (2007a). Adhesion analysis of multi-level hierarchical attachment systems contacting with a rough surface. *J. Adhesion Sci.*, **21**(1):1–20.

Kim, T. W. and Bhushan, B. (2007b). Effects of stiffness of multi-level hierarchical attachment system on adhesion enhancement. *Ultramicroscopy*, **107**:902–912.

Kim, T. W. and Bhushan, B. (2008). The adhesion model considering capillarity for gecko attachment system. *J. R. Soc. Interface*, **5**:319–327.

Klarbring, A. (1991). Derivation of a model of adhesively bonded joints by the asymptotic expansion method. *Int. J. Engng. Sci.*, **29**(4):493–512.

Klarbring, A. and Movchan, A. B. (1998). Asymptotic modelling of adhesive joints. *Mech. Mater.*, **28**:137–145.

Kočvara, M., Mielke, A., and Roubiček, T. (2006). A rate-independent approach to the delamination problem. *Math. Mech. Solids*, **11**(4):423–447.

Komvopoulos, K. (2003). Adhesion and friction forces in microelectromechanical systems: mechanisms, measurement, surface modification techniques, and adhesion theory. *J. Adhes. Sci. Tech.*, **17**(4):477–517.

Krull, H. and Yuan, H. (2011). Suggestions to the cohesive tractionseparation law from atomistic simulations. *Engrg. Frac. Mech.*, **78**:525–533.

Kwaki, J. S. and Kim, T. W. (2010). A review of adhesion and friction models for gecko feet. *Int. J. Precis. Eng. Manuf.*, **11**(1):171–186.

Landman, U., Luedtke, W. D., Burnham, N. A., and Colton, R. J. (1990). Atomistic mechanisms and dynamics of adhesion, nanoindentation, and fracture. *Science*, **248**(4954):454–461.

Lane, M. (2003). Interface fracture. *Annu. Rev. Mater. Res.*, **33**:29–54.

Laursen, T. A. (2002). *Computational Contact and Impact Mechanics: Fundamentals of modeling interfacial phenomena in nonlinear finite element analysis*. Springer.

Leffler, K., Alfredsson, K. S., and Stigh, U. (2007). Shear behaviour of adhesive layers. *Int J. Solids Struct.*, **44**:530–545.

Li, F., Pan, J., and Sinka, C. (2011a). Modelling adhesive contact between fine particles using material point method. *Mech. Mater.*, **43**:157–167.

Li, Q. and Kim, K.-S. (2009). Micromechanics of rough surface adhesion: A homogenized projection method. *Acta Mech. Solida Sinica*, **22**(5):377–390.

Li, Q. Y. and Yu, S. W. (2004). A model for computational investigation of elasto-plastic normal and tangential contact considering adhesion effect. *Acta Mech. Sinica*, **20**(2):165–171.

Li, S., Marshall, J. S., Liu, G., and Yao, Q. (2011b). Adhesive particulate flow: The discrete-element method and its application in energy and environmental engineering. *Prog. Ener. Combust. Sci.*, **37**:633–668.

Li, S., Thouless, M. D., Waas, A. M., Schroeder, J. A., and Zavattieri, P. D. (2006). Mixed-mode cohesive-zone models for fracture of an adhesively bonded polymer-matrix composite. *Engng. Frac. Mech.*, **73**(1):64–78.

Li, S., Wang, J., and Thouless, M. D. (2004). The effects of shear on delamination in layered materials. *J. Mech. Phys. Solids*, **52**:193–214.

Liljedahl, C. D. M., Crocombe, A. D., Wahab, M. A., and Ashcroft, I. A. (2005). The effect of residual strains on the progressive damage modelling of environmentally degraded adhesive joints. *J. Adhes. Sci. Technol.*, **19**(7):525–547.

Lin, Y. and Freund, L. B. (2007). Forced detachment of a vesicle in adhesive contact with a substrate. *Int. J. Solids Struc.*, **44**:1927–1938.

Lin, Y. Y., Hui, C. Y., and Wang, Y. C. (2002). Modeling the failure of an adhesive layer in a peel test. *J. Polymer Sci. B - Polymer Phys.*, **40**(19):2277–2291.

Lin, Y.-Y. and Wu, M.-H. (2012). Analysis on adhesive contact of micro-columns. *J. Adhes.*, **88**:86–107.

Lion, A. and Höfer, P. (2007). On the phenomenological representation of curing phenomena in continuum mechanics. *Arch. Mech.*, **59**(1):59–89.

Lipowsky, R. and Seifert, U. (1991). Adhesion of membranes: A theoretical perspective. *Langmuir*, **7**:1867–1873.

Liu, G., Li, S., and Yao, Q. (2010). On the applicability of different adhesion models in adhesive particulate flows. *Front. Energy Power Eng. China*, **4**(2):280–286.

Liu, P., Zhang, J. W., Cheng, Q. H., and Lu, C. (2007). Simulations of the spreading of a vesicle on a substrate surface mediated by receptor-ligand binding. *J. Mech. Phys. Solids*, **55**:1166–1181.

Liu, P. F. and Zheng, J. Y. (2010). Recent developments on damage modeling and finite element analysis for composite laminates: A review. *Materials & Design*, **31**(8):3825–3834.

Liu, T., Liu, G., Xie, Q., and Wang, Q. J. (2006). An EFG-FE coupling method for microscale adhesive contacts. *J. Tribol.-T. ASME*, **128**(1):40–48.

Loh, W. K., Crocombe, A. D., Wahab, M. A., and Ashcroft, I. A. (2003). Modelling interfacial degradation using interfacial rupture elements. *J. Adhesion*, **79**:1135–1160.

Long, R. and Hui, C.-Y. (2012). Axisymmetric membrane in adhesive contact with rigid substrates: Analytical solutions under large deformation. *Int. J. Solids Struc.*, **49**:672–683.

Long, R., Shull, K. R., and Hui, C.-Y. (2010). Large deformation adhesive contact mechanics of circular membranes with a flat rigid substrate. *J. Mech. Phys. Solids*, **58**(9):1225–1242.

Lorentz, E. (2008). A mixed interface finite element for cohesive zone models. *Comput. Methods Appl. Mech. Engrg.*, **198**:302–317.

Lu, Z. X., Yu, S. W., Wang, X. Y., and Feng, X. Q. (2007). Effect of interfacial slippage in peel test: Theoretical model. *Eur. Phys. J. E*, **23**:67–76.

Luan, B. and Robbins, M. O. (2006). Contact of single asperities with varying adhesion: Comparing continuum mechanics to atomistic simulations. *Phys. Rev. E*, **74**(2):026111.

Lubowiecka, I., Rodriguez, M., Rodriguez, E., and Martinez, D. (2012). Experimentation, material modelling and simulation of bonded joints with a flexible adhesive. *Int. J. Adhesion Adhesives*, **37**:56–64.

Luding, S. (2008). Cohesive, frictional powders: contact models for tension. *Granular Matter*, **10**(4):235–246.

Ma, L., McMeeking, R., and Arzt, E. (2007). Adhesive contact between flat punches with finite edge radius and an elastic half-space. *Int. J. Mat. Res.*, **98**(11):1156–1162.

Martiny, P., Lani, F., Kinloch, A. J., and Pardoen, T. (2008). Numerical analysis of the energy contributions in peel tests: A steady-state multilevel finite element approach. *Int J. Adhesion Adhesives*, **28**:222–236.

Matous, K., Kulkarni, M. G., and Geubelle, P. H. (2008). Multiscale cohesive failure modeling of heterogeneous adhesives. *J. Mech. Phys. Solids*, **56**(4):1511–1533.

Maugis, D. (1987). Adherence of elastomers: Fracture mechanics aspects. *J. Adhes. Sci. Technol.*, **1**((2)):105–134.

Maugis, D. (1992). Adhesion of spheres: The JKR-DMT transition using a Dugdale model. *J. Colloid Interface Sci.*, **150**(1):243–269.

Maugis, D. (1996). On the contact and adhesion of rough surfaces. *J. Adhes. Sci. Technol.*, **10**((2)):161–175.

McGarry, J. P., Murphy, B. P., and McHugh, P. E. (2005). Computational mechanics modelling of cell-substrate contact during cyclic substrate deformation. *J. Mech. Phys. Solids*, **53**:2597–2637.

Medina, S. and Dini, D. (2014). A numerical model for the deterministic analysis of adhesive rough contacts down to the nano-scale. *J. Solids Struct.*, **51**:2620–2632.

Mergel, J. C. and Sauer, R. A. (2014). On the optimum shape of thin adhesive strips for various peeling directions. *J. Adhesion*, **90**(5-6):526–544.

Mergel, J. C., Sauer, R. A., and Saxena, A. (2014). Computational optimization of adhesive microstructures based on a nonlinear beam formulation. *Struc. Multidiscipl. Optim.*, **50**(6):1001–1017.

Mergheim, J., Possart, G., and Steinmann, P. (2012). Moidelling and computation of curing and damage of thermosets. *Comp. Mat. Sci.*, **53**(1):359–367.

Mesarovic, S. D. and Johnson, K. L. (2000). Adhesive contact of elastic-plastic spheres. *J. Mech. Phys. Solids*, **48**:2009–2033.

Moës, N., Dolbow, J., and Belytschko, T. (1999). A finite element method for crack growth without remeshing. *Int. J. Numer. Meth. Eng.*, **46**:131–150.

Molinari, A. and Ravichandran, G. (2008). Peeling of elastic tapes: Effects of large deformations, pre-straining, and of a peel-zone model. *J. Adhesion*, **84**:961–995.

Mróz, Z. and Stupkiewicz, S. (1998). Constitutive model of adhesive and ploughing friction in metal-forming processes. *Int. J. Mech. Sci.*, **40**(2-3):281–303.

Muller, V. M., Yushchenko, V. S., and Derjaguin, B. V. (1980). On the influence of molecular forces on the deformation of an elastic sphere and its sticking to a rigid plane. *J. Colloid Interface Sci.*, **77**:91–101.

Nadler, B. and Tang, T. (2008). Decohesion of a rigid punch from non-linear membrane undergoing finite axisymmetric deformation. *Int. J. Non-lin. Mech.*, **43**:716–721.

Namilae, S. and Chandra, N. (2005). Multiscale model to study the effect of interfaces in carbon nanotube-based composites. *J. Engrg. Mater. Technol.*, **127**:222–232.

N'Dri, N. A., Shyy, W., and Tran-Son-Tay, R. (2003). Computational modelling of cell adhesion and movement using a continuum-kinetics approach. *Biophys. J.*, **85**:2273–2286.

Nesemann, L. and Stephan, E. P. (2012). Numerical solution of an adhesion problem with fem and bem. *Appl. Numer. Math.*, **62**(5):606–619.

Nguyen, D., Rasmuson, A., Thalberg, K., and Björn, I. N. (2014). Numerical modelling of breakage and adhesion of loose fine-particle agglomerates. *Chem. Eng. Sci.*, **116**:91–98.

Ogden, R. W. (1987). *Non-Linear Elastic Deformations*. Dover.

Ono, K. (2012). Numerical method of analyzing contact mechanics between a sphere and a flat considering lennard-jones surface forces of contacting asperities and noncontacting rough surfaces. *J. Tribology*, **134**(1):011402.

Orr, F. M., Scriven, L. E., and Rivas, A. P. (1975). Pendular rings between solids: meniscus properties and capillary force. *J. Fluid. Meth.*, **67**(4):723–742.

Ortiz, M. and Pandolfi, A. (1999). Finite-deformation irreversible cohesive elements for three-dimensional crack-propagation analysis. *Int. J. Numer. Meth. Engng*, **44**:1267–1282.

Ouyang, Z. and Li, G. (2009). Nonlinear interface shear fracture of end notched flexure specimens. *Int. J. Solids Struct.*, **46**:2656–2668.

Oyharcabal, X. and Frisch, T. (2005). Peeling of an elastica from a smooth attractive substrate. *Phys. Rev. E*, **71**:036611.

Padday, J. F. (1971). The profiles of axially symmetric menisci. *Proc. Roy. Soc. A*, **269**(1197):265–293.

Paggi, M. and Wriggers, P. (2011). A nonlocal cohesive zone model for finite thickness interfaces – Part I: Mathematical formulation and validation with molecular dynamics. *Comput. Mater. Sci.*, **50**:1625–1633.

Pakarinen, O. H., Foster, A. S., Paajanen, M., Kalinainen, T., Katainen, J., Makkonen, I., Lahtinen, J., and Nieminen, R. M. (2005). Towards an accurate description of the capillary force in nanoparticle-surface interactions. *Model. Simul. Mater. Sci. Eng.*, **13**:1175–1186.

Paliwal, B. and Cherkaoui, M. (2013). An improved atomistic simulation based mixed-mode cohesive zone law considering non-planar crack growth. *Int. J. Solids Struct.*, **50**:3346–3360.

Pantano, A., Pugno, N. M., and Gorb, S. N. (2011). Numerical simulations demonstrate that the double tapering of the spatualae of lizards and insects maximize both detachment resistance and stability. *Int. J. Fracture*, **171**(2):169–175.

Pathak, A., Deshpande, V. S., McMeeking, R. M., and Evans, A. G. (2008). The simulation of stress fibre and focal adhesion development in cells on patterned substrates. *J. R. Soc. Interface*, **5**:507–524.

Peri, M. D. M. and Cetinkaya, C. (2009). Spherical nanoparticle-substrate adhesion interaction simulations utilizing molecular dynamics. *J. Adhes. Sci. Tech.*, **23**(13-14):1723–1738.

Persson, B. N. J. (2001). Theory of rubber friction and contact mechanics. *J. Chem. Phys.*, **115**(8):3840–3861.

Persson, B. N. J. (2002). Adhesion between an elastic body and a randomly rough hard surface. *Eur. Phys. J. E*, **8**:385–401.

Persson, B. N. J. (2003). On the mechanism of adhesion in biological systems. *J. Chem. Phys.*, **118**(16):7614–7621.

Persson, B. N. J., Albohr, O., Tartaglino, U., Volokitin, A. I., and Tosatti, E. (2005). On the nature of surface roughness with application to contact mechanics, sealing, rubber friction and adhesion. *J. Phys. Condens. Matter*, **17**(3):R1–R62.

Persson, B. N. J. and Tosatti, E. (2001). The effect of surface roughness on the adhesion of elastic solids. *J. Chem. Phys.*, **115**(12):5597–5610.

Pesika, N. S., Tian, Y., Zhao, B., Rosenberg, K., Zeng, H., McGuiggan, P., Autumn, K., and Israelachvili, J. N. (2007). Peel-zone model of tape peeling based on the gecko adhesive system. *J. Adhesion*, **83**:383–401.

Point, N. and Sacco, E. (1996a). A delamination model for laminated composites. *Int. J. Solids Struc.*, **33**(4):483–509.

Point, N. and Sacco, E. (1996b). Delamination of beams: An application to the dcb specimen. *Int. J. Frac.*, **79**(3):225–247.

Qu, L., Dai, L., Stone, M., Xia, Z., and Wang, Z. L. (2008). Carbon nanotube arrays with strong shear binding-on and easy normal lifting-off. *Science*, **322**:238–242.

Quesnel, D. J. and Rimai, D. S. (2000). Finite element modeling of particle adhesion: A surface energy formalism. *J. Adhesion*, **74**(1-4):177–194.

Radhakrishnan, H. and Mesarovic, S. D. (2009). Adhesive contact of elastic spheres revisited: numerical models and scaling. *Proc. Roy. Soc. A*, **465**:2231–2249.

Rahulkumar, P., Jagota, A., Bennison, S. J., and Saigal, S. (2000). Cohesive element modeling of viscoelastic fracture: application to peel testing of polymers. *Int. J. Solids Struc.*, **37**(13):1873–1897.

Raous, M., Cangémi, L., and Cocu, M. (1999). A consistent model coupling adhesion, friction, and unilateral contact. *Comput. Methods Appl. Mech. Engrg.*, **177**:383–399.

Roe, K. L. and Siegmund, T. (2003). An irreversible cohesive zone model for interface fatigue crack growth simulation. *Eng. Frac. Mech.*, **70**(2):209–232.

Rojek, J. and Telega, J. J. (1999). Numerical simulation of bone-implant systems using a more realistic model of the contact interfaces with adhesion. *J. Theor. Appl. Mech.*, **37**(3):659–686.

Rojek, J. and Telega, J. J. (2001). Contact problems with friction, adhesion and wear in orthopaedic biomechanics. I. General developments. *J. Theor. Appl. Mech.*, **39**(3):555–577.

Rojek, J., Telega, J. J., and Stupkiewicz, S. (2001). Contact problems with friction, adhesion and wear in orthopaedic biomechanics. II. Numerical implementation and application to implanted knee joints. *J. Theor. Appl. Mech.*, **39**(3):679–706.

Roy, S., Darque-Ceretti, E., Felder, E., and Monchoix, H. (2007). Cross-sectional nanoindentation for copper adhesion characterization in blanket and patterned interconnect structures: experiments and three-dimensional fem modeling. *Int. J. Fracture*, **144**:21–33.

Sahoo, P. (2006). Adhesive friction for elastic-plastic contacting rough surfaces considering asperity interaction. *J. Phys. D: Appl. Phys.*, **39**(13):2809–2818.

Salgado, N. K. and Aliabadi, M. H. (1998). The boundary element analysis of cracked stiffened sheets, reinforced by adhesively bonded patches. *Int. J. Numer. Meth. Engrg.*, **42**(2):195–217.

Samimi, M., van Dommelen, J. A. W., and Geers, M. G. D. (2009). An enriched cohesive zone model for delamination in brittle interfaces. *Int. J. Numer. Meth. Engrg.*, **80**(5):609–630.

Sancaktar, E. (2011). Constitutive adhesive and sealant models. In da Silva, L. F. M., Öchsner, A., and Adams, R. D., editors, *Handbook of Adhesion Technology*, pages 553–595. Springer.

Sanz-Herrera, J. A. and Reina-Romo, E. (2011). Cell-biomaterial mechanical interaction in the framework of tissue engineering: Insights, computational modeling and perspectives. *Int. J. Molec. Sci.*, **12**(11):8217–8244.

Sauer, R. A. (2006). *An atomic interaction based continuum model for computational multiscale contact mechanics*. PhD thesis, University of California, Berkeley, USA.

Sauer, R. A. (2009a). A computational contact model for nanoscale rubber adhesion. In Heinrich, G., Kaliske, M., Lion, A., and Reese, S., editors, *Constitutive Models for Rubber VI*, pages 47–52. Taylor & Francis Group.

Sauer, R. A. (2009b). Multiscale modeling and simulation of the deformation and adhesion of a single gecko seta. *Comp. Meth. Biomech. Biomed. Engng.*, **12**(6):627–640.

Sauer, R. A. (2010). A computational model for nanoscale adhesion between deformable solids and its application to gecko adhesion. *J. Adhes. Sci. Technol.*, **24**:1807–1818.

Sauer, R. A. (2011a). Challenges in computational nanoscale contact mechanics. In Müller-Hoeppe, D., Löhnert, S., and Reese, S., editors, *Recent Developments and Innovative Applications in Computational Mechanics*, pages 39–46. Spinger.

Sauer, R. A. (2011b). Enriched contact finite elements for stable peeling computations. *Int. J. Numer. Meth. Engrg.*, **87**:593–616.

Sauer, R. A. (2011c). The peeling behavior of thin films with finite bending stiffness and the implications on gecko adhesion. *J. Adhes.*, **87**(7-8):624–643.

Sauer, R. A. (2013). Local finite element enrichment strategies for 2D contact computations and a corresponding postprocessing scheme. *Comput. Mech.*, **52**(2):301–319.

Sauer, R. A. (2014a). Advances in the computational modeling of the gecko adhesion mechanism. *J. Adhes. Sci. Technol.*, **28**(3-4):240–255.

Sauer, R. A. (2014b). A contact theory for surface tension driven systems. *Math. Mech. Solids*, published online, DOI: 10.1177/1081286514521230.

Sauer, R. A. (2014c). Stabilized finite element formulations for liquid membranes and their application to droplet contact. *Int. J. Numer. Meth. Fluids*, **75**(7):519–545.

Sauer, R. A. and De Lorenzis, L. (2013). A computational contact formulation based on surface potentials. *Comput. Methods Appl. Mech. Engrg.*, **253**:369–395.

Sauer, R. A. and Holl, M. (2013). A detailed 3D finite element analysis of the peeling behavior of a gecko spatula. *Comp. Meth. Biomech. Biomed. Engng.*, **16**(6):577–591.

Sauer, R. A. and Li, S. (2007a). An atomic interaction-based continuum model for adhesive contact mechanics. *Finite Elem. Anal. Des.*, **43**(5):384–396.

Sauer, R. A. and Li, S. (2007b). A contact mechanics model for quasi-continua. *Int. J. Numer. Meth. Engrg.*, **71**(8):931–962.

Sauer, R. A. and Li, S. (2008). An atomistically enriched continuum model for nanoscale contact mechanics and its application to contact scaling. *J. Nanosci. Nanotech.*, **8**(7):3757–3773.

Sauer, R. A. and Mergel, J. C. (2014). A geometrically exact finite beam element formulation for thin film adhesion and debonding. *Finite Elem. Anal. Des.*, **86**:120–135.

Sauer, R. A. and Wriggers, P. (2009). Formulation and analysis of a 3D finite element implementation for adhesive contact at the nanoscale. *Comput. Methods Appl. Mech. Engrg.*, **198**:3871–3883.

Schargott, M. (2009). A mechanical model of biomimetic adhesive pads with tilted and hierarchical structure. *Bioinsp. Biomim.*, **4**:026002.

Schmidt, M. G., Sauer, R. A., and Ismail, A. E. (2014). Multiscale treatment of mechanical contact problems involving thin polymeric layers. *Modelling Simul. Mater. Sci. Eng.*, **22**:045012.

Schmidt, P. and Edlund, U. (2006). Analysis of adhesively bonded joints: a finite element method and a material model with damage. *Int. J. Numer. Meth. Engng.*, **66**(1271-1308).

Schmidt, P. and Edlund, U. (2010). A finite element method for failure analysis of adhesively bonded structures. *Int. J. Adhesion Adhesives*, **30**(665-681).

Schubert, B., Majidi, C., Groff, R. E., Baek, S., Bush, B., Maboudian, R., and Fearing, R. S. (2007). Towards friction and adhesion from high modulus micofiber arrays. *J. Adhesion Sci. Technol.*, **21**(12-13):1297–1315.

Scott, M. A., Borden, M. J., Verhoosel, C. V., Sederberg, T. W., and Hughes, T. J. R. (2011). Isogeometric finite element data structures based on Bézier extraction of T-splines. *Int. J. Numer. Meth. Engng.*, **88**(2):126–156.

Shavezipur, M., Li, G. H., Laboriante, I., Gou, W. J., Carraro, C., and Maboudian, R. (2011). A finite element technique for accurate determination of interfacial adhesion force in MEMS using electrostatic actuation. *J. Micromech. Microeng.*, **21**:115025.

Simo, J. C. and Hughes, T. J. R. (1998). *Computational Inelasticity*. Springer.

Sofonea, M., Arhab, R., and Tarraf, R. (2006a). Analysis of electroelastic frictionless contact problems with adhesion. *J. Appl. Math.*, **2006**:1–25.

Sofonea, M., Han, W., and Shillor, M. (2006b). *Analysis and Approximation of Contact Problems with Adhesion and Damage*. Chapman & Hall/CRC, Boca Raton.

Sørensen, B. (2002). Cohesive law and notch sensitivity of adhesive joints. *Acta Materialia*, **50**:1053–1061.

Spenko, M. J., Haynes, G. C., Saunders, J. A., Cutkosky, M. R., Rizzi, A. A., Full, R. J., and Koditschek, D. E. (2008). Biologically inspired climbing with a hexapedal robot. *J. Field Robotics*, **25**(4-5):223–242.

Sriwijaya, R. R. A., Jatmiko, K., and Takahashi, K. (2007). An analytical approach for the adhesion of a semi-infinite elastic body in contact with a sinusoidal rigid surface under zero external pressure. *J. Adhesion Sci. Technol.*, **21**(10):899–909.

Stapleton, S., Pineda, E. J., Gries, T., and Waas, A. M. (2014). Adaptive shape functions and internal mesh adaptation for modeling progressive failure in adhesively bonded joints. *Int. J. Solids Struct.*, **51**:3252–3264.

Streator, J. L. and Jackson, R. L. (2009). A model for the liquid-mediated collapse of 2-D rough surfaces. *Wear*, **267**(9-10):1436–1445.

Su, C., Wei, Y. J., and Anand, L. (2004). An elastic-plastic interface constitutive model: application to adhesive joints. *Int. J. Plast.*, **20**(12):2063–2081.

Suh, A. Y., Yu, N., Lee, K. M., Polycarpou, A. A., and Johnson, H. T. (2004). Crystallite coalescence during film growth based on improved contact mechanics adhesion models. *J. Appl. Phys.*, **96**(3):1348–1359.

Suresh, S. (1998). *Fatigue of Materials*. Cambridge University Press, Cambridge.

Tadmor, R. (2001). The London–van der Waals interaction energy between objects of various geometries. *J. Phys. Condens. Matter*, **13**:L195–L202.

Talon, C. and Curnier, A. (2003). A model of adhesion coupled to contact and friction. *Eur. J. Mech. A*, **22**:545–565.

Tang, M. and Soh, A. (2011). Simulation of a bio-adhesion system with viscoelasticity. In Ariffin, A., Abdullah, S., Ali, A., Muchtar, A., Ghazali, M., and Sajuri, Z., editors, *Key Engineering Materials*, volume **462-463**, pages 780–784. Trans Tech Publications.

Tang, T., Hui, C.-Y., and Glassmaker, N. J. (2005). Can a fibrillar interface be stronger and tougher than a non- fibrillar one? *J. R. Soc. Interface*, **2**:505–516.

Thouless, M. D. and Yang, Q. D. (2008). A parametric study of the peel test. *Int. J. Adhesion Adhesives*, **28**:176–184.

Timoshenko, S. P. and Goodier, J. N. (1970). *Theory of Elasticity*. McGraw-Hill, 3rd edition.

Touzaline, A. (2010). Analysis of a quasistatic contact problem with adhesion and nonlocal friction for viscoelastic materials. *Appl. Math. Mech. - Engl. Ed.*, **31**(5):623–634.

Tozeren, A., Sung, K.-L. P., and Chien, S. (1989). Theoretical and experimental studies on cross-bridge migration during cell disaggregation. *Biophys. J.*, **55**:479–487.

Tran, P., Kandula, S. S. V., Geubelle, P. H., and Sottos, N. R. (2008). Hybrid spectral/finite element analysis of dynamic delamination of patterned thin films. *Engrg. Frac. Mech.*, **75**(14):4217–4233.

Tsang, P. H., Li, G., Brun, Y. V., Freund, L. B., and Tang, J. X. (2006). Adhesion of single bacterial cells in the micronewton range. *Proc. Natl. Acad. Sci.*, **103**:5764–5768.

Tvergaard, V. (1990). Effect of fiber debonding in a whisker-reinforced metal. *Mater. Sci. Engng.*, **125**:203–213.

Tvergaard, V. and Hutchinson, J. W. (1992). The relation between crack growth resistance and fracture process parameters in elastic-plastic solids. *J. Mech. Phys. Solids*, **40**:1377–1397.

Tworzydlo, W. W., Cecot, W., Oden, J. T., and Yew, C. H. (1998). Computational micro- and macroscopic models of contact and friction: formulation, approach and applications. *Wear*, **220**(2):113–140.

van den Bosch, M. J., Schreurs, P. J. G., and Geers, M. G. D. (2006). An improved description of the exponential Xu and Needleman cohesive zone law for mixed-mode decohesion. *Engng. Fract. Mech.*, **73**:1220–1234.

Verhoosel, C. V., Scott, M. A., de Borst, R., and Hughes, T. J. R. (2011). An isogeometric approach to cohesive zone modeling. *Int. J. Numer. Meth. Engng.*, **87**(1-5):336–360.

Vossen, B. G., Schreurs, P. J. G., van der Sluis, O., and Geers, M. G. D. (2014). Multi-scale modeling of delamination through fibrillation. *J. Mech. Phys. Solids*, **66**:117–132.

Wan, K.-T. and Julien, S. E. (2009). Confined thin film delamination in the presence of inter-surface forces with finite range and magnitude. *J. Appl. Mech.*, **76**(5):051005.

Wang, W. and King, M. R. (2012). Multiscale modeling of platelet adhesion and thrombus growth. *Ann. Biomed. Engng.*, **40**(11):2345–2354.

Wei, Y. (2004). Modeling nonlinear peeling of ductile thin filmscritical assessment of analytical bending models using FE simulations. *Int. J. Solids Struct.*, **41**:5087–5104.

Wei, Y. (2014). A stochastic description on the traction-separation law of an interface with non-covalent bonding. *J. Mech. Phys. Solids*, **70**:227–241.

Wei, Y. and Hutchinson, J. W. (1998). Interface strength, work of adhesion and plasticity in the peel test. *Int. J. Fracture*, **93**:315–333.

Weissenfels, C. (2013). *Contact methods integrating plasticity models with application to soil mechanics*. PhD thesis, Leibniz University Hannover, Hannover, Germany.

White, S. R. and Hahn, H. T. (1992). Process modeling of composite-materials – residual-stress development during cure: 1. Model formulation. *J. Compos. Mater.*, **26**(16):2402–2422.

Williams, J. A. and Kauzlarich, J. J. (2005). The influence of peel angle on the mechanics of peeling flexible adherends with arbitrary load-extension characteristics. *Tribol. Int.*, **38**:951–958.

Williams, J. G. (1993). Root rotation an plastic work effects in the peel test. *J. Adhesion*, **41**:225–239.

Wong, H. C. and Tang, W. C. (2011). Finite element analysis of the effects of focal adhesion mechanical properties and substrate stiffness on cell migration. *J. Biomech.*, **44**(6):1046–1050.

Wriggers, P. (2006). *Computational Contact Mechanics*. Springer, 2$^{\text{nd}}$ edition.

Wriggers, P. (2008). *Nonlinear Finite Element Methods*. Springer.

Wriggers, P. and Reinelt, J. (2009). Multi-scale approach for frictional contact of elastomers on rough rigid surfaces. *Comput. Methods Appl. Mech. Engrg.*, **198**(21-26):1996–2008.

Wu, G. and Crocombe, A. D. (1996). Simplified finite element modelling of structural adhesive joints. *Comput. Struct.*, **61**(2):385–391.

Wu, J.-J. (2006). Adhesive contact between a nano-scale rigid sphere and an elastic half-space. *J. Phys. D: Appl. Phys.*, **39**:351–358.

Wu, J.-J. (2008). Easy-to-implement equations for determining adhesive contact parameters with the accuracy of numerical simulations. *Tribol. Lett.*, **30**:99–105.

Xu, X.-P. and Needleman, A. (1993). Void nucleation by inclusion debonding in a crystal matrix. *Model. Simul. Mater. Sci. Engng.*, **1**(2):111–132.

Yadagiri, S., Reddy, C. P., and Reddy, T. S. (1987). Viscoelastic analysis of adhesively bonded joints. *Comput. Struct.*, **27**(4):445–454.

Yamakov, V., Saether, E., Phillips, D. R., and Glaessgen, E. H. (2006). Molecular-dynamics simulation-based cohesive zone representation of intergranular fracture processes in aluminum. *J. Mech. Phys. Solids*, **54**:1899–1928.

Yang, C., Tartaglino, U., and Persson, B. N. J. (2006). A multiscale molecular dynamics approach to contact mechanics. *Eur. Phys. J. D*, **19**(1):47–58.

Yang, Q. D., Thouless, M. D., and Ward, S. M. (1999). Numerical simulations of adhesively-bonded beams failing with extensive plastic deformation. *J. Mech. Phys. Solids*, **47**(6):1337–1353.

Yao, H. and Gao, H. (2006). Mechanics of robust and releasable adhesion in biology: Bottom-up designed hierarchical structures of gecko. *J. Mech. Phys. Solids*, **54**:1120–1146.

Yao, H. and Gao, H. (2007). Bio-inspired mechanics of bottom-up designed hierarchical materials: robust and releasable adhesion systems of gecko. *Bulletin of the Polish Academy of Sciences - Technical Sciences*, **55**(2):141–150.

Yong, C. W., Kendall, K., and Smith, W. (2004). Atomistic studies of surface adhesions using molecular-dynamics simulations. *Phil. Trans. R. Soc. Lond. A*, **362**:1915–1929.

Yongsheng, L., Yuanzhong, H., and Linqing, Z. (1999). Adhesive contact of flat-ended wedges: Theory and computer experiments. *Transactions of the ASME*, **121**:128.

Yu, H., Adams, R. D., and da Silva, L. F. M. (2013). Development of a dilatometer and measurement of the shrinkage behaviour of adhesives during the cure process. *Int. J. Adhesion Adhesives*, **47**:26–34.

Yurdumakan, B., Raravikar, N. R., Ajayan, P. M., and Dhinojwala, A. (2005). Synthetic gecko foot-hairs from multiwalled carbon nanotubes. *Chem. Commun.*, **30**:3799–3801.

Zeng, X. and Li, S. (2011). Modelling and simulation of substrate elasticity sensing in stem cells. *Comp. Meth. Biomech. Biomed. Engng.*, **14**(5):447–458.

Zhang, C. Y. and Zhang, Y. W. (2008). Computational analysis of adhesion force in the indentation of cells using atomic force microscopy. *Phys. Rev. E*, **77**:021912.

Zhang, C.-Z. and Wang, Z.-G. (2008). Nucleation of membrane adhesions. *Phys. Rev. E*, **77**:021906.

Zhang, J., Das, S., and Du, Q. (2009). A phase field model for vesicle-substrate adhesion. *J. Comp. Phys.*, **228**:7837–7849.

Zhang, J., Zhao, Z., and Wei, X. (2010). A damage cohesive model for simulating 90° peel propagation in anisotropic conductive bonding. In Zhang, L. C., Zhang, C. L., and Shi, T. L., editors, *Advanced Materials Research*, volume **139-141**, pages 374–377.

Zhang, X., Zhang, X., and Wen, S. (2011). Finite element modeling of the nano-scale adhesive contact and the geometry-based pull-off force. *Tribol. Lett.*, **41**:65–72.

Zhao, X., Adams, R. D., and da Silva, L. F. M. (2011a). Single lap joints with rounded adherend corners: Experimental results and strength prediction. *J. Adhes. Sci. Technol.*, **25**(8):837–856.

Zhao, X., Adams, R. D., and da Silva, L. F. M. (2011b). Single lap joints with rounded adherend corners: Stress and strain analysis. *J. Adhes. Sci. Technol.*, **25**(8):819–836.

Zhao, Y.-P., Wang, L. S., and Yu, T. X. (2003). Mechanics of adhesion in MEMS – a review. *J. Adhesion Sci. Technol.*, **17**(4):519–546.

Zheng, J. and Streator, J. L. (2004). A liquid bridge between two elastic half-spaces: A theoretical study of interface instability. *Tribol. Lett.*, **16**(1-2):1–9.

Zhou, X. W., Moody, N. R., Jones, R. E., Zimmerman, J. A., and Reedy, E. D. (2009). Molecular-dynamics-based cohesive zone law for brittle interfacial fracture under mixed loading conditions: Effects of elastic constant mismatch. *Acta Materialia*, **57**:4671–4686.

Zhu, C. (2000). Kinetics and mechanics of cell adhesion. *J. Biomech.*, **33**:23–33.

Zienkiewicz, O. C. and Taylor, R. L. (2005). *The Finite Element Method for Solid and Structural Mechanics*. Butterworth-Heinemann, 6$^{\text{th}}$ edition.

Zienkiewicz, O. C., Taylor, R. L., and Zhu, J. Z. (2005). *The Finite Element Method: Its basis and fundamentals*. Butterworth-Heinemann, 6$^{\text{th}}$ edition.

Zilberman, S. and Persson, B. N. J. (2002). Adhesion between elastic bodies with rough surfaces. *Solid State Communications*, **123**:173–177.

Zmitrowicz, A. (2010). Contact stresses: a short survey of models and methods of computations. *Arch. Appl. Mech.*, **80**(12):1407–1428.